Geochemical investigation of electrical conductivity and electrical double layer based wettability alteration during engineered water injection in carbonates

DOI:
10.1016/j.petrol.2022.110627

Journal of Petroleum Science and Engineering 215 (2022) 110627
https://doi.org/10.1016/j.petrol.2022.110627

Geochemical Investigation of Electrical Conductivity and Electrical Double Layer based Wettability Alteration during Engineered Water Injection in Carbonates

Ilyas Khurshid*, Imran Afgan

Khalifa University of Science and Technology, Abu Dhabi, 127799, UAE.

*Corresponding author. Tel.: +971566198515;

E-mail address: ilyas.khurshid@ku.ac.ae

Abstract

The injection of engineered water to increase the oil recovery from carbonates is increasingly becoming popular due to its reduced environmental impact and low cost of operation. However, the related variation in electric properties of rock and fluid with this technique is still ambiguous and needs thorough investigation. This study explores the variation in electrical conductivity, ion mobility, electrical double layer thickness, and the related oil recovery with the change in water composition from a geochemical perspective. In this study, we implemented the improved wettability alteration model based on the variation in electrical conductivity with a Matlab-IPhreeqc coupled simulator, to model the electrical conductivity, ion mobility, and electrical double layer (EDL) thickness. The variation in concentration of the ionic species obtained from the geochemical model is used to determine the electrical conductivity. This electrical conductivity-based wettability modification is dynamically simulated in the transport model. The model is validated with experimental coreflood data conducted on carbonates by simulating the electrical conductivity measurements reported in the literature. From the findings, it is evident that the formation temperature, sulfate concentration, and dilution of injected seawater have a noticeable effect on electrical conductivity during engineered water injection. In addition, EDL thickness is the main parameter affected by the change in electrical conductivity. In addition, it is suggested to inject high-temperature water in carbonate reservoirs because it would increase ion mobility. This increase in ion mobility would enhance the EDL thickness and water film would be stabilized. Moreover, seawater dilution would decrease electrical conductivity while spiking of sulfate concentration would increase the activity of sulfate ions. However, the concentration of sulfate ions should be controlled as a wettability alteration agent, as it could cause the formation and precipitation of calcium sulfate. Furthermore, the variation in electrical conductivity and EDL thickness caused by the injection of seawater and diluted seawater increased the recovery of oil by approximately 16-21% in the selected case study.

1. Introduction

Several core flooding experiments of engineered water injection into the carbonate core samples reported an increase in the recovery of oil (Khurshid and Al-Shalabi, 2022). A number of these experiments were performed to pinpoint the underlying mechanisms responsible for the recovery of oil. Different measurements such as contact angle, atomic force microscopy, core flooding, and spontaneous imbibition were executed at molecular to core scale to determine the effect of engineered water injection in carbonates (Taheriotaghsara *et al.,* 2020). Strand *et al.* (2006) and Zhang *et al.* (2007) investigated the effect of increasing temperature and the concentration of potential determining ions in the injected water. They observed that additional oil could be recovered from oil-wet carbonates by increasing temperature and the content of sulfate in the injected water. After performing a number of experiments on carbonates, Fathi *et al.* (2011) recovered additional oil from oil-wet carbonate rock by reducing the concentration of sodium chloride in the injected water. Yousef *et al.* (2011); Chandrasekhar and Mohanty (2013) and Chandrasekhar *et al.* (2018) injected seawater and various recipes of diluted seawater in carbonates and calculated the increase in the recovery of oil. Similarly, to analyze the effect of engineered water injection at a large scale, single-well chemical tracer injection, and real oil fields, pilot test injections were performed to evaluate the impact

of engineered water injection (Al-Shalabi and Sepehrnoori, 2017). Moreover, Seccombe *et al.* (2010) were the first to report the engineered water injection in inter-well application in Endicott field, Alaska. They reported a reduction in the residual oil saturation, which was also in agreement with the coreflooding experiment and single well-tests. However, for a North Sea oil field (Snorre oil field) the injection of engineered water resulted in no additional oil recovery. Moreover, Mahani *et al.* (2011) investigated the performance of engineered water injection in a couple of fields in Syria. For one of the oil fields, they observed an improvement in oil recovery in the secondary mode but no recovery when engineered water was injected in the tertiary mode. This success/failure during fluid injection is attributed to reservoir rock pore collapse and fracturing (Khurshid *et al.*, 2015), and related formation damage (Khurshid *et al.,* 2018) rather than the recovery mode.

In carbonate, the mechanism behind the wettability alteration with the injection of engineered water is still debatable/uncertain. By engineered waterflooding, we refer to the injection of water that has attuned ionic composition. In the past, several researchers have performed both experimental measurement and numerical simulations to study the mechanism behind wettability alteration by the injected engineered water. Mahani *et al.* (2015 and 2017), investigated the various electrokinetic properties of different carbonate rocks. They found that with the injection of engineered water, the charge at the rock-oil-brine interface changes polarity (from positively charged to negatively charged). Khurshid and Al-Shalabi (2022) found that the charge at the rock-oil-brine interface weakens, where the positivity and negativity decreases. Thus, engineered water injection leads to the phenomena of electrical double layer (EDL) expansion at the rock-oil-brine interface (Nasralla *et al.*, 2016; Mahani *et al.*, 2017). This mechanism was considered as the cause of wettability modification in carbonates. The dissolution of calcite was proposed by Hiorth *et al.* (2010) after performing geochemical modeling. They mentioned that calcite dissolution is responsible for the wettability alteration in carbonates. However, through micro-CT images using chemical trace analysis, Ouden (2014) observed that formation dissolution has an insignificant effect in altering formation porosity. In another study, Yousef *et al.* (2011) used a nuclear magnetic resonance test for carbonates (middle-east formations). They detected pore connectivity increase, after the injection of engineered water and found that the dissolution of a certain mineral (anhydride) could improve the connectivity of pores leading to improvement in oil recovery. The ionic exchange was proposed by Purswani and Karpyn, (2019) as a mechanism responsible for wettability modification in carbonates. Additionally, several researchers investigated the significance of the formation brine and the effect of its pH on the wettability alteration by utilizing the bond product sum (BPS) concept (Brady and Thyne, 2016; Chen *et al.*, 2018; Xie *et al.*, 2018). Recently, Khurshid and Afgan (2021a) and Khurshid *et al.* (2020) found that the injection of engineered water (sulfate spiking) could cause formation damage with the formation and precipitation of anhydrite and it could decrease the recovery of oil.

Therefore, it is important to mention that the difference in various described interpretations of the perceived wettability modification in carbonates represents, the disagreement in understanding the principal mechanism for controlling the engineered waterflooding effect in carbonates. Although a number of researchers investigated the various mechanisms responsible for the wettability modification. However, it is important to highlight that all the suggested mechanisms play an important role in oil recovery during the injection of engineered water. Because the various mechanisms are correlated and could influence each other. Such as, the dissolution of carbonate could change the composition of water that could initiate a change in pH (Ouden, 2014; Chandrasekhar *et al.,* 2018). These modifications could affect the electrostatic forces used for the estimation of BPS (Brady and Thyne, 2016; Xie *et al.*, 2018; Sari *et al.,* 2019) that lead to wettability modification. In addition, the variation in the composition of the formation brine could modify the electrokinetics at the rock-oil-brine interface (Mahan *et al.,* 2017, Khurshid and Al-Shalabi 2022). This impacts the EDL thickness at the rock-oil-brine interface. It is important to mention that the increase or decrease in the concentration of potential determining ions due to formation dissolution and/or ion exchange not only affects the zeta potential but also the thickness of the EDL (Kasha *et al.*, 2015; Abdallah *et al.*, 2014). Yousef *et al.* (2011) performed an XRD analysis of various carbonate reservoir rocks and reported that

anhydride dissolution in carbonates could increase sulfate concentration in the effluent concentration and could enhance ionic exchange that is considered responsible for the wettability alteration process (Austad *et al.,* 2015). Consequently, in true essence, the combination of various mechanisms should be investigated together.

To characterize the electrokinetic interactions at rock-oil-brine surfaces, it is important to state that carbonate surface groups and oil (carboxylic acid group and nitrogen base group) act as charged particles in the porous media and interact with the various injected ionic species present in the injected engineered water. Thus, with the injection of engineered water, the electrical conductivity could change causing the electrical double layer to expand because of the decrease in ionic concentration along with the rock-oil-brine interface. This multi-layer is composed of co-ions (same charge) and counter ions (opposite charge). **Fig. 1** presents the schematic diagram for the formation of an electrical double layer around the carbonate surface. It is evident from the figure that the EDL formed along the surface of carbonate is made up of two layers: stern layer and diffused layer. Moreover, beyond the diffused layer, the ions can move freely in the bulk fluid. The carbonates are mostly composed of calcite when they interact with ionic species present in the reservoir fluid (brine). This results in the formation of various speciation sites in the stern layer with calcium (Ca^{2+}) and carbonate (CO_3^{2-}) present in calcite. The stern layer is further subdivided into three sub-layers: (i) hydrolysis layer, (ii) Inner Helmholtz plane (IHP) and (iii) the outer Helmholtz plane (OHP). It is assumed that the surface potential at the surface of carbonate up to the OHP is constant as shown in **Fig.1**. However, after the OHP, carbonate potential (electrical) reduces exponentially (Tetteh *et al.*, 2022). Away from the OHP, lies the diffused layer and it consists of freely moving ions (co-ions and counter-ions). The presence of potential determining ions such as SO_4^{2-}, Mg^{2+}, Ca^{2+} in this region ensures that the EDL remains electrically neutral. Moreover, in the stern layer the ions such as Na^+, K^+, and Cl^- are considered inactive species. These inactive ions could also form a layer that stabilizes the stern layer, allowing the measurement of a stable electrical potential (Alotaibi and Yousef, 2017; Alotaibi *et al.,* 2018). Udoh and Vinogradov (2019) measured the variation in electrical conductivity with the injection of engineered water in carbonates. However, it is important to incorporate the variation in electrical conductivity with the multiphase flow. This requires the coupling of a geochemical package with a multiphase flow simulator to understand the dynamic effects of change in electrical conductivity on the wettability modification and related oil recovery.

There have been several attempts to relate the wettability alteration response to engineered water injection. Korrani *et al.* (2016) assumed that the total ionic strength is responsible for the alteration of wettability during engineered water injection. However, their suggested model due to its inherent simplicity was not able to predict the detrimental effect of divalent ions on oil recovery. Brady and Thyne (2016), and Qiao et al. (2015) coupled the surface-based reactions between the components of rock and oil. For this, generally, a detailed demonstration/understanding of the variation in electric conductivity and various geochemical species controlling it are required. It is thus important to characterize different geochemical species, various reactions, and their corresponding wettability modification in multiphase-flow models. Moreover, the existing geochemical models lack the capability to link the electric conductivity, relative permeability, and associated recovery of oil. In this study, we, therefore, predict the recovery of oil under different water compositions, carbonate rocks characteristics, and variation in electrical conductivity. It is important to mention that various multicomponent reactive transport models were developed as early as the 1980s and have been utilized to investigate different subsurface reactive-transport processes in many applications (Qiao *et al.*, 2015). From a geochemistry point of view, the use of these complex models is promising. However, the effect of the change in electric conductivity in EOR processes needs detailed investigation to characterize the effect of electrical conductivity. In this research, a novel model is developed that couples multiphase flow and the variation of electric conductivity for the first time. Thus, the suggested approach has the capability to systematically examine the complex interactions at the microscopic level to predict wettability alteration, and oil recovery. The integrated framework is developed for carbonates based on the variation in electric conductivity. The results obtained from the new model were compared with the engineered

water experimental data. It was observed that both the rock and fluid properties (porosity, permeability, and relative permeability) and the geochemical reactions (aqueous- and dissolution/precipitation reactions) play an important role. Thus, we performed several simulations with the suggested technique under an array of conditions to understand the parameters controlling electrical conductivity, ionic strength, and the thickness of EDL with the injection of engineered water.

This research study is organized as follows. In section 1, the general multiphase-flow and reactive-transport equations are introduced. Then in section 2, we focused on the model development and its validation with the experimental data. After that, in section 3 the reaction network is presented that discusses the relationship between various geochemical species, electric conductivity, and relative permeability including the sensitivity analysis of the important parameters. Finally, in section 4, the effect of electrical conductivity on oil recovery is discussed.

2. Model Development and Description

The Phreeqc is a geochemical computer program designed to simulate a wide variety of geochemical calculations in subsurface aqueous flow. During engineered water injection in an oil field, we usually encounter multiphase flow where more than one phase (oil and water) flows simultaneously through the porous media. However, Phreeqc can simulate only the single-phase, and thus it could not be used to model the effect of geochemistry in multiphase flow in petroleum reservoirs. Therefore, we used IPhreeqc instead of Phreeqc in coupling because IPhreeqc provides an application programming interface to facilitate coupling with other programs like Matlab and python. The description of IPhreeqc-Matlab coupling to investigate the effect of electrical conductivity by the injection of engineered water on oil recovery is presented as follows.

2.1. Multiphase Phase (Oil and Water) Flow. The conservation equations of mass and momentum were combined to describe the flow of two fluids that are immiscible in the subsurface porous medium. The derived mass conservation equation for each phase of these fluids is set as follow (Bear, 2013):

$$\frac{\partial}{\partial t}\phi\rho_i S_i(x,t) + \nabla . q_i(x,t)\rho_i = 0\ . \tag{1}$$

In deriving these equations, it is assumed that the two fluids are incompressible and their density (ρ) remains constant. We present the fluid momentum conservation by Darcy's law and it is presented by:

$$q_i(x,t) = -\frac{A\,k(x)\,k_{ri}(S_i)}{\mu_i}[\nabla p_i(x,t) + \rho_i g], \tag{2}$$

where $q(x, t)$ represents the production of phase i, $k(x)$ is representing the reservoir permeability, $k_{ri}(S_i(x, t))$ stands for relative permeability for phase i controlled by the saturation, $p_i(x, t)$ is the pressure of phase i, and the saturation of all phases is summed equal to 1.

$$S_1 + S_2 = 1, \tag{3}$$

Moreover, the capillary pressure is given by the differences of pressure of each phase by the following equation:

$$P_c(S) = P_1 - P_2. \tag{4}$$

From the various boundary conditions of fluid incompressibility and mass conservation, the divergence of the total fluid $q(x, t) = q_1(x, t) + q_2(x, t)$ is found to be zero and it is given by

$$\nabla . q(x,t) = 0\ . \tag{5}$$

The above equations from 1-5 are combined to form :

$$\phi \frac{\partial S(x,t)}{\partial t} + \frac{\partial}{\partial S}[\psi(S)(q(x,t) + k(x)\lambda_2(S)g\Delta\rho)].\nabla S(x,t) = \nabla.[\psi(S)k(x)\lambda_2(S)\frac{dp_c(S)}{dS}\nabla S(x,t)]. \quad (6)$$

where *ψ(S)* is the function of fluid fractional flow and it is presented by:

$$\psi(S) = \frac{\lambda_1(S)}{\lambda_1(S)+\lambda_2(S)}, \quad (7)$$

where λ is the mobility of the fluid phase and which defines the ratio of phase relative permeability to its viscosity. The equation of Buckley-Leverette displacement is utilized to solve the two fluids that are immiscible during the process of engineered water injection and oil production. After the incorporation of **Equation (6)**, the following equation is used (Bear, 2013):

$$\phi \frac{\partial S(x,t)}{\partial t} + \frac{d\psi(S)}{dS} q(x,t).\nabla S(x,t) = 0, \quad (8)$$

where the chemical species and its concentration is calculated by the equation as follows (Khurshid *et al.*, 2020).

$$\phi \frac{\partial [S(x,t),C_\gamma(x,t)]}{\partial t} + \frac{d[\psi(S),C_\gamma(x,t)]}{dS} q(x,t).\nabla S(x,t) = 0. \quad (9)$$

where the concentration of geochemical species is presented by *C* and subscript γ represent the type of ionic specie.

It is important to mention here that in the past a number of researchers have successfully coupled IPhreeqc with reservoir simulators. De Bruin (2012) coupled IPhreeqc with a transport code, Shell's in-house reservoir simulator MPRS was coupled with IPhreeqc by Wei (2012), and it was later expended by Farajzadeh *et al.* (2012) for mechanical modeling of Alkaline-Surfactant-Polymer (ASP) flooding. Korrani (2014) coupled UTCHEM and IPhreeqc to model reactive transport problems during waterflooding. Recently, Boampong *et al.* (2021) built a triple-layer surface complexation model in Phreeqc and coupled it with UTCHEM and Khurshid *et al.* (2022a) estimated the surfactant adsorption in carbonates under harsh conditions using the surface complexation modeling. By coupling IPhreeqc and Matlab, we incorporated all capabilities of base code Phreeqc such as speciation calculation, saturation-index calculations, and transport calculation with both reversible and irreversible reactions. This includes aqueous reactions, solid-solution reactions, ion-exchange equilibria, kinetically controlled reactions. Thus, by coupling, all the above-mentioned features of Phreeqc are incorporated in the developed multiphase flow simulator. This technique successfully simulates the reactive transport in a porous formation.

Fig. 2 shows the flowchart of the reactive multiphase model with IPhreeqc-Matlab coupled simulator. First, the equation of mass conservation is solved in Matlab, after that the geochemical inputs are incorporated in the computer memory using the AccumulateLine command, then the geochemical engine is executed using the RunAccumulated command to determine the new state of equilibrium. All the results are transferred from IPhreeqc to Matlab by using the GetSelectedOutputValue command. The IPhreeqc uses the Davies equation or the Extended Debye-Huckel equation to calculate the activity coefficients which is given as follow:

Davies Equation (Parkhurst and Appelo, 2013)

$$log\gamma_i = -Az_i^2\left[\frac{\sqrt{I}}{1+\sqrt{I}} - 0.3I\right], \quad (10)$$

Extended Debye-Huckel Equation (Parkhurst and Appelo, 2013)

$$log\gamma_i = -\frac{Az_i^2\sqrt{I}}{1+Ba_i^0\sqrt{I}} + b_i I, \quad (11)$$

where γ represents coefficient for ions activity, *A* and *B* are the constants dependent on temperature, *I* is the solution ionic strength and it is determined by:

$$I = \frac{1}{2} \sum_{i=1}^{n} m_i (z_i)^2 \, . \quad (12)$$

The IPhreeqc uses the van't Hoff equation to calculate the equilibrium constants dependency on temperature. The equation is given as:

$$LogK_T = LogK_{298} - \frac{\Delta H^0_{r\,298}}{2.3025R} [\frac{1}{T} - \frac{1}{298.15}] \, , \quad (13)$$

where *K* stands for equilibrium constant, ΔHr represents the change in system enthalpy, *R* is the universal gas constant. It is possible to calculate the solid mineral solubility products dependent on the system pressure and it is given by the following equation:

$$LogK_P = LogK_{P=1} - \frac{\Delta V_r}{2.303RT} (P - 1) \, , \quad (15)$$

where *P* represents the system pressure in atm and ΔV_r shows the volume change (cm^3/mol).

2.2. Changes in Electric Conductivity. The electrical conductivity of brine is related to the concentration of ionic species present in the formation brine. The dissolved salts and inorganic solids species such as alkalis, carbonates, chloride, and sulfate compounds are the sources of ionic species. They dissociate into positively (cations) and negatively charged (anions) ions. The high concentration of these ions results in increased conductivity of brine/water and vice versa. Moreover, deionized or distilled water could act as an insulator because of its negligible conductivity. It is important to mention that seawater has very high electrical conductivity because the average TDS of seawater is 35,000- 40,000 ppm. To determine the electrical conductivity of a solution, first, the summation of different ions is calculated separately, as different ionic species have different molar conductivity (Λ_m). The following equation is used to determine the molar conductivity (Appelo and Postma, 2005):

$$\Lambda_m = \sigma_i / m_i, \quad (16)$$

Where σ_i stands for electrical conductivity (Siemens/m, S/m) due to the contribution of ionic species *i* with a concentration of m_i (mol/L). Thus, the electrical conductivity of an aqueous solution is calculated by multiplying the ionic species conductivity with the concentration of ionic species (mmol/L) and summing them up.

After determining the electrical conductivity, it is important to measure the Debye length because it is an important property of an interfacial double layer and serves as an instrument to measure the thickness of the double-layer. It was observed that by decreasing ionic strength, the Debye length increases, making the electrical double layer (EDL) thicker. Thus, an increase in Debye length would stabilize the water film due to the presence of strong electrostatic interactions. It is suggested to determine the Debye length by using the conductivity measurements as mentioned by Dukhin and Goetz (2012). It can be calculated from the solution electrical conductivity by the following equation

$$\kappa^{-1} = \sqrt{\frac{\varepsilon D}{\sigma}} \quad (17)$$

where ε is the dielectric permittivity and *D* is the diffusion coefficient.

2.3. Model Validation/Justification

The simulation of geochemical interaction in porous media is a complex modeling technique because it requires the equilibrium phase of reservoir rock, formation water compositions, injected water compositions, formation thermodynamic conditions, rate of fluid injection, temperature, and pressure. Thus, to validate the developed geochemical model. We analyzed all these parameters, examined and provided input to the developed simulator. The section below presents the validation of the developed model with: (1) single-phase flow scale precipitation

modeling, (2) comparison of the developed IPhreeqc-Matlab coupled simulator with fluid displacement equation (Buckley-Leverette), (3) Eclipse (commercial simulator), and (4) electrical conductivity experimental data.

2.3.1. Validation with Phreeqc. This section of the paper presents the validation of the IPhreeqc-Matlab coupled simulator with the Phreeqc. We used the experimental data of Khormali *et al.* (2016) single-phase scale precipitation corefloods data, modeled and compared it with the IPhreeqc-Matlab coupled simulator and Phreeqc. The Phreeqc is used for the single-phase reactive transport model because it is the state-of-the-art geochemical engine (Parkhurst and Appelo, 2013). Phreeqc's capabilities of modeling reactive transport are well recognized and acknowledged by academia and industry. Thus, we compared the validation of the developed IPhreeqc-Matlab coupled simulator against Phreeqc. The various inputs for formation water and seawater composition, and rock properties are provided in **Table 1-2**. The comparisons of the effluent concentration of different ionic species with both simulators are shown in **Figs. 3 - 14**.

***2.3.1.1 Comparison of Aqueous species*.** The details of carbonate composition, its lithology, various elements, grid dimensions, and different details used in the simulation runs are listed in **Table 2**. The comparisons between Phreeqc and IPhreeqc-Matlab coupled simulator regarding the various aqueous species as well as pH are presented in **Figs. 3 – 8**. It is evident from the results that all the ionic species such as sodium, chloride, calcium, magnesium, sulfate as well the pH are a good match.

2.3.1.2 Comparison of Solid Species. The molar concentration of different solid species such as calcite, dolomite, and kaolinite as well as those solid species formed (anhydrite) due to the geochemical interaction of injected seawater, carbonate rock, and formation water are presented in **Figs. 9 – 11**. The molar concentrations of different solid species obtained by Phreeqc are compared against the IPhreeqc-Matlab coupled simulator. The initial concentration of different solids before the injection of seawater is shown in **Fig. 9**. It is important to mention that the default concentration of calcite, dolomite, and kaolinite was kept at 10 moles in the simulations because solid moles have an insignificant effect and the mineral solubility is comparatively very low (Parkhurst and Appelo, 2013). It is evident from **Fig. 9** that the anhydrite initial concentration is zero because primarily, it was not present in the carbonate core sample. However, it precipitates when it becomes supersaturated. The concentration of various solid species after the injection of 6 PVs of seawater is presented in **Fig. 10**. Moreover, the concentrations of solid species for the first grid block at the end of seawater injection are depicted in **Fig. 11**. The results show that the prediction of solid species concentrations is in good agreement between the Phreeqc and IPhreeqc-Matlab coupled simulator at both the start and end of the seawater injection.

2.3.1.3 Comparison of Ion-Exchange Species. The carbonate composition is presented in **Table 2** and it shows that the concentration of clay is just 7%, thus it is important to compare the concentration of ion exchange species in the simulation. **Figs. 12 – 15** depicts the concentration of various ion-exchangers such as NaX, KX, CaX_2, and MgX_2 using both IPhreeqc-Matlab coupled simulator and Phreeqc at the start and end of the seawater injection. The various ion exchange reactions with their coefficient of selectivity can be found in Phreeqc.dat while the composition of injected seawater and formation water used in the simulation is presented in **Table 1**.

2.3.2. Validation with Buckley-Leverette Displacement Equation. The Buckley-Leverette displacement equation is well known for estimating the fluid displacement and its dynamics by the injected fluid. It is used to investigate the immiscible displacement and the flow of incompressible fluid. Thus, the results of the developed IPhreeqc-Matlab coupled simulator are validated against the Buckley-Leverette displacement equation. The purpose is to confirm that the developed IPhreeqc-Matlab coupled simulator determines the oil and water flow dynamics and the recovery of oil. The saturation profile of water across the simulated model at various injected pore volumes is shown in **Fig. 16.** It can be observed from this figure that the two simulators are in a good match, thus confirming the effectiveness of the developed IPhreeqc-Matlab coupled simulator.

2.3.3. Validation with Eclipse-100 (Commercial Simulator). We used Eclipse-100, a commercial simulator to confirm the ability of the IPhreeqc-Matlab coupled simulator to characterize the injection of engineered water. We examined the various features of the IPhreeqc-Matlab using interpolation of injected fluid salinity for two sets of relative permeability and capillary pressure. The different inputs can be found elsewhere in Khurshid *et al.* (2020). **Fig. 17** shows the results of the IPhreeqc-Matlab coupled simulator. It is evident from the oil recovery data that the commercial simulator and our developed model are in good agreement. This comparison demonstrates the capability of the IPhreeqc-Matlab coupled simulator in capturing the effects of engineered water injection.

2.3.4. Validation with Electrical Conductivity and pH Experimental Data. The experimental work performed by Udoh and Vinogradov, (2019) was used to investigate the capabilities of the IPhreeqc-Matlab coupled simulator to determine electrical conductivity and pH. We selected core C-27, a carbonate core, and sequence 4 from Udoh and Vinogradov, (2019) experimental work for validation. This experiment was performed on carbonate rock at a temperature of 70 °C for which the various properties and compositions of the core used in the geochemical modeling are presented in **Table 3-4**. The concentration of different ions and charge balance for different injected waters is provided in **Table 3**. It can be observed that the concentration of total dissolved solids in the formation brine and engineered water was varied between 141,149 and 429 ppm, respectively. It is important to mention that we used *Pitzer.dat* database in this study because this database has distinct features to simulate high-salinity water effects. To match Udoh and Vinogradov, (2019) data, the parameters that were tuned were dispersivity, coefficient of diffusion, and coefficient of thermal diffusion as listed in **Table 4.**

It is essential to mention that in the simulations, the engineered water was injected into a carbonate rock that was composed of 95% calcite, 4% dolomite, and 1% anhydrite, at a temperature of 70 ^{o}C. The electrical conductivity and pH experimental data from Udoh and Vinogradov, (2019) were used to compare the modeling results as depicted in **Figs. 18 and 19**. It can be observed from these figures that the pH measurements of the experimental data and simulation results are in good agreement. Moreover, from the results presented in **Fig. 18** it is evident that with the injection of engineered water, the electrical conductivity of the formation decreases from 281 mS/cm to 7 mS/cm at 70 °C.

Fig. 19 illustrates the influence of engineered water on pH. It is apparent from the results that the initial pH of the formation water which was 7, increases to 8, where it gets stabilized with the continuous injection of engineered water. Moreover, it is also evident from the profile of pH presented in **Fig. 19** that the pH of the aqueous phase is affected by the change in ionic strength and this would perturb the electrical conductivity for the whole formation. This finding proves, that with the injection of engineered water, the electrical conductivity would decrease and the pH would increase as shown in **Figs. 18** and **19**. It is mentioned by Al-Shalabi *et al.* (2015) and Al-Shalabi and Sepehrnoori, (2017) that an increase in pH causes a significant change in the surface charge which results in expansion of the electrical double layer. Thus, the observed increase in pH and decrease in electrical conductivity is controlling the wettability alteration. It can be concluded from these results that the electrical conductivity decreases with the injection of engineered water and this decrease leads to the increase of EDL thickness and water film stabilization. Further explanation of the change in electrical conductivity will be presented in the results and discussion section. It is prudent to mention here that the decrease in electrical conductivity has a noticeable impact on the oil recovery from the reservoir. Moreover, we performed a sensitivity analysis of various grids and found that a model with 20 grids successfully captured the geochemical phenomena and the related electrical conductivity variation.

3. Results and Discussion

An integrated framework is developed to simulate the variation of electrical conductivity as presented in the previous sections of this research study. We investigated the effect of temperature of different injected waters, the

concentration of sulfate, and the dilution of seawater on electrical conductivity. We kept the values of different parameters within the typical range of reservoir conditions as shown in **Tables 3-5**. We ran all the simulations for 10 pore volumes, determined the variation in electrical conductivity and electrical double layer for the last grid block. It is imperative to mention that we selected the last grid block because the injected engineered water would displace the formation water and would react with the formation solid species. Thus, it is the best approach to analyze the concertation of different ionic species in the effluent. Moreover, the effluent analysis would assist to determine the cumulative change in electrical conductivity, EDL thickness, and related wettability alteration due to engineered water injection.

3.1. Injected Water Temperature Effect. The influence of injected seawater temperature on electrical conductivity, ionic strength, and EDL is explored in this subsection of the paper. Usually, the activity of an ionic species is a better predictor of its response to the change in thermodynamic conditions than its concentration. **Figs. 20-22** present the effect of temperature on electrical conductivity, ionic strength, and comparison with EDL. Electrical conductivity and ionic strength are considered to be co-dependent parameters. However, temperature affects the electrical conductivity of a solution by increasing its ionic mobility. This finding is evident from **Fig. 20** that with the increase in temperature, the electrical conductivity increases. Thus, when the temperature of formation is 70°C its electrical conductivity is 29 S/m. However, when the temperature of the formation increases first to 90°C and then to 110°C, its electrical conductivity increases to 36 S/m and 41 S/m, respectively. It is important to mention that the composition of the formation water and seawater were kept constant as shown in **Table 5**.

Fig. 21 shows the effect of temperature on ionic strength. It can be observed from **Fig. 21** that temperature has no effect on the ionic strength of the solution. Thus, measuring the electrical double layer based on ionic strength could result in an erratic estimation of EDL as ionic strength is the concentration of all ionic species present in the brine and its concentration remains the same when the temperature is changed. However, the increase or decrease in temperature changes the ion mobility as it is affected by the kinetic energy of the solution. The kinetic energy affects the ion mobility of ions and counter ions, which would categorically affect the thickness of the electrical double layer. Therefore, the estimation of EDL should be based on the mobility of ions along with the ionic concentration, ignoring ion mobility results in erratic estimation as stated above. Based on these findings, it is thus suggested that the EDL thickness should be compared with electrical conductivity rather than ionic strength.

The comparison of electrical conductivity and EDL thickness is shown in **Fig. 22.** In this study, we measured both the electrical conductivity and EDL thickness at 5 PV as the profile stabilizes at this point. It is evident from the results presented in **Fig. 22** that for seawater injection both the electrical conductivity and EDL thickness increase with temperature for example at 70°C the electrical conductivity is 11.94 S/m which increases to 14.54 S/m at 90°C and 17.12 S/m at 110°C. A similar trend is observed for the EDL thickness. Thus, it is concluded that both the electrical conductivity and EDL thickness are directly related to the temperature of the formation.

3.2. Sulfate Concentration Effect. The effect of sulfate concentration on electrical conductivity at 90 °C is presented in **Fig. 23.** The findings from the previous subsections showed that kinetic energy and ion mobility are important factors that control the EDL thickness. If the temperature of the formation is low, the kinetic energy and ion mobility decrease, and thus the EDL thickness would be low, leading to the formation of a thin water film during the injection of engineered water. Therefore, we performed a detailed sensitivity analysis to understand the effect of sulfate concentration on electrical conductivity, ionic strength, and EDL thickness. In **Fig. 23**, the concentration of sulfate in the base case is kept constant at 0.024 mol/L, shown as the blue curve. The concentration of sulfate was varied including two-times spiked (0.048 mol/L), two-times diluted (0.012 mol/L), and four-times diluted (0.006 mol/L). It is important to mention that we tuned the concentration of Cl^- and Na^+ as these two species are inactive. Moreover, we kept the concentration of total dissolved solids in all spiked and diluted sulfate water similar to the seawater (38,580 ppm) as shown in **Table 5**. Additionally, the boundary conditions, formation temperature, injected water temperature, reservoir permeability, and porosity were all kept constant.

Figs. 23 and 24 show the electrical conductivity and ionic strength profile for different engineered waters. It is apparent from these two figures that all these injected engineered waters have the same profile. The behavior of ionic strength is the same. However, one can observe some differences in the behavior of electrical conductivity. Moreover, for the spiked and various diluted sulfate water injection cases at 5 PV of engineered water injection, we observed a significant variation in electrical conductivity and EDL thickness as shown in **Fig. 25**. The figure indicates that the electrical conductivity is controlled by the mobility of ionic species (sulfate in this specific case of water injection). It can also observed that with the injection of seawater, various spiked, and diluted water resulted in a significant increase in EDL thickness. For formation water, the EDL thickness remained at 0.162 nm, but it increased to 0.326 nm for seawater, 0.324 nm for two-times spiked seawater, and 0.328 nm for two-times diluted seawater. Thus, our finding proves the recommendation of previous researchers that the injection of spiked/diluted sulfate concentration is a good approach to improve the oil recovery in carbonates (Strand *et al*., 2006; Zhang *et al*., 2007; Chandrasekhar and Mohanty, 2013). Thus, the sulfate concentration in the injected water should be modified to increase the recovery of oil but at the same time, it is necessary to reduce the formation damage caused by the formation and precipitation of anhydrite as suggested by Khurshid *et al.* (2020). Therefore, the coupled effect of sulfate spiking and dilution on electrical conductivity and the recovery of oil is presented later in this study. Moreover, it is indispensable to mention that the effect of temperature, sulfate spiking, and dilution are consistent in presenting the significance of electrical conductivity and EDL thickness.

3.3. Effect of Water Dilution. We analyzed the impact of seawater and injection of its various diluted recipes on electrical conductivity, ionic strength, and EDL thickness in this subsection of the paper. The results are presented in **Figs. 26-28**. The ionic compositions of seawater and its various diluted compositions are shown in **Table 5.** The different diluted seawater includes two-times diluted (19,290 ppm), 10-times diluted (3,858 ppm), 20-times diluted (1,929 ppm), and 100-times diluted (386 ppm). **Fig. 26** presents the base case of seawater injection as an orange curve. The total dissolved solids in seawater are 38,580 ppm and it causes the least decrease in electrical conductivity from 35.28 S/m to 14.54 S/m at 5.0 PV of seawater injection. However, when this seawater is diluted, we can observe a further reduction of 8.56, 2.95, 2.31, and 1.66 S/m for two-times diluted, 10-times diluted, 20-times diluted, and 100-times diluted, respectively. We also observed similar behavior for the ionic strength variation in **Fig. 27**. Moreover, the comparison of electrical conductivity and EDL thickness (as shown in **Fig. 28**), reveals that the EDL thickness increases from 0.162 nm for formation water to 0.322 nm for seawater, 0.43 nm for two-times, 0.72 for ten-times, 0.79 nm for twenty-times and 0.90 nm for hundred-times diluted seawater. It is prudent to mention here that the injection of hundred-times diluted seawater is the most effective water recipe in increasing the thickness of EDL, and water film stabilization.

4. Effect of Electrical Conductivity on Oil Recovery. In carbonate, the maximum oil can be recovered with the injection of CO_2 at supercritical conditions (Khurshid and Choe 2016; Khurshid and Fujii, 2021; Khurshid and Afgan 2021b) but it could cause the precipitation/deposition of asphaltene, dissolution of carbonate particles and cementation of asphaltene and dissoluted particles (Khurshid and Choe, 2015; Khurshid *et al.,* 2020); sludge formation (Khurshid *et al.,* 2022b). The injection of water does not cause the formation damages and can successfully maintain reservoir pressure. However, if formation water is re-injected it usually results in no additional oil recovery. The injection of engineered water results in enhanced oil recovery because its injection reduces the formation electrical conductivity and ionic strength, thereby increasing the EDL thickness thus assists in the release of bonded oil from the formation. Moreover, the injection of engineered water in clay-rich formations such as sandstones would lead to the desorption of adsorbed cations on the clay surface. This desorption of cations would rupture the bond between clay surface and organic material (carboxylic acid group). This process will assist in separating the oil blobs attached to the surface of the clay. Therefore, the wettability would change to a more water-wet state (Khurshid and Al-Shalabi, 2022).

However, carbonates have insignificant clay concentration, the injection of engineered water in carbonates would lead to a sharp decrease in the concentration of all the ionic species. Thus, the electrical conductivity that is

the product of ion mobility and ion concentration would decrease. This decrease in electrical conductivity is different from the reduction in ionic strength because ionic strength only depends on the ionic concentration. Electrical conductivity has an ion mobility factor that is distinct for different ionic species which changes with the thermodynamic conditions of the reservoir. Thus, with the injection of engineered water, the decrease in electrical conductivity would increase the thickness of the electrical double layer, and the water film would become stabilized. This stabilization of the water film would lead to the release of the bonded oil. However, it is worth mentioning that it is not possible to regulate the thickness of EDL and the stabilization of the water film. However, one could adjust the composition of the water that is injected into the reservoir.

After the injection of engineered water, the electrical conductivity decreases. It is evident from **Fig. 26** that the electrical conductivity that was initially at 35 S/m decreased to 14.18 S/m with the injection of seawater at 90°C. This is a 60% decrease in electrical conductivity. Moreover, the injected water is seawater that is rich in sulfate with 0.024 mol/L and formation water has a sulfate concentration of just 0.004 mol/L. Thus, with the injection of seawater, the concentration of species such as calcium, magnesium, sodium, and chloride decrease but sulfate concentration increases as shown in **Table 5**. Moreover, the decrease in electrical conductivity would lead to a drop in the positive surface charge of the carbonate. This decrease in the positive surface charge would help in the adsorption of more calcium ions on the carbonate surface. This process would lead to a decrease in the electrostatic repulsion force, increase in the EDL thickness, thereby accelerating the interaction of calcium ions with the carboxylic acid group (Zhang *et al.*, 2007). The chemical reaction is given by the following equation:

$$Ca^{2+} + SO_4^{2-} + RCOO^- - Ca - CaCO_3(s) \rightleftharpoons RCOO^- - Ca^+ + Ca - CaCO_3(s) + SO_4^{2-} . \quad (18)$$

Thus, with the decrease in electrical conductivity, the sulfate ions would play the role of a catalyst and stimulate the activity of Ca^{2+} ions close to the carbonate surface (Strand *et al.*, 2006; Lager *et al.*, 2007). It is important to mention that this reaction would only occur when the electrical conductivity is decreased. This process would increase the thickness of EDL and thus the carbonate's positive charged surface would be enhanced. Thus, the negatively charged sulfate ions would adsorb on these carbonate sites, leading to the release of bonded oil ganglions. After detailed modeling of different parameters such as temperature, the concentration of sulfate and water dilution, and their effect on electrical conductivity as shown in **Figs. 20-28,** it is evident that when the temperature of the injected water is high, the ion mobility increases due to the increase in kinetic energy of the ionic species. Furthermore, the high mobility of sulfate ions is shown for the two-times sulfate spike case in **Fig. 25.** The results confirm that during the injection of sulfate spiked engineered water, the sulfate ions because of their high mobility would play the role of a catalyst (**Equation 18**). This mechanism of decrease in electrical conductivity is utilized in the developed Matlab-IPhreeqc coupled simulator. This is because electrical conductivity and repulsion forces are the main sources of increase in Debye length and water film thickness because of engineered water injection as previously presented in **Figs. 22, 25,** and **28**.

We simulated different cases of water injection to examine the variation in the electrical conductivity and its impact on the recovery of oil with the injection of seawater, spiking/dilution of sulfate, and water dilution. Chandrasekhar and Mohanty (2018) injected engineered water and history matched the ionic concentration of various species, measured pressure drop, oil recovery, to estimate the relative permeability. In their experiment, the fluid flow governing law such as Darcy's law and related steady-state flow conditions were assumed to be applicable. They determined the various relative permeability parameters such as Corey's exponents and endpoints. The oil relative permeability (K_{ro}) was estimated from the ratio of effective permeability of fluid to absolute permeability of the reservoir and the water relative permeability (K_{rw}) was determined by utilizing Darcy's law. The values obtained were 0.123 (K_{ro}), 0.02 (K_{rw}), 3.30 (n_o), and 2.55 (n_w). It is evident from **Fig. 29** that the water and oil relative permeability curves intersected at 0.42 (water saturation). The details of the different parameters for this mixed-wet carbonate core are presented in **Table 6**. The term mixed-wet is used to define a formation that has heterogeneous wettability because the formation grains have non-uniform wettability due to different sizes of pores

in the formation. The small formation pores are water-wet and the large formation pores are oil-wet (Ejeh *et al*., 2020).

Here, the change in electrical conductivity is presented as a wettability modifier with the injection of seawater and ten-times diluted seawater. The results show that the variation of electrical conductivity is the controlling parameter that affects EDL thickness and is responsible for the stabilization of the water film. Therefore, for the simulations, the variation in electrical conductivity is considered through an interpolating parameter, ω, which presents the modification of formation wettability from oil-wet/ mixed-wet to water-wet. The concept of applying the interpolating parameter for engineered water injection was utilized by a number of researchers in the past including Jerauld *et al.* (2008), Ligthelm *et al*. (2009), Xie *et al.* (2014), Sanaei *et al*. (2018), Korrani and Jerauld (2019) and Khurshid *et al.* (2020).

The variation in electrical conductivity is integrated as an interpolating parameter by the following equation:

$$\omega(x,t) = \frac{\lambda_{max} - \lambda(x,t)}{\lambda_{max} - \lambda_{min}},\ 0 \le \omega \le 1\ , \tag{19}$$

where λ_{max} is the initial/ maximum electrical conductivity at formation brine with the trivial impact of engineered water injection, $\lambda(x,t)$ is the electrical conductivity at x,t representing position and time, respectively. The λ_{min} is the minimum electrical conductivity below which engineered water has an insignificant effect. **Equation (19)** determines the value of ω (interpolating parameter) between the relative permeability curves from an oil-wet/mixed oil-wet to a water-wet. We performed a detailed analysis for this specific case study and after several simulations, it was found that λ_{max}, the value above which the engineered water effect is negligible is when the electrical conductivity is 323 S/m (in-situ formation electrical conductivity). On the other hand, λ_{min}, the value below which the engineered water has no effect is zero S/m because at this condition the injected water will be deionized water with least/zero ionic species. Therefore, during engineered water injection the change in $\omega(x,t)$ is represented by **Equation (19)** that considers the $\lambda(x,t)$ value in each grid and at each time step. Thus, before the injection of engineered water, the ω is 0 and oil-wetting conditions persist as $\lambda(x,t) = \lambda_{max}$. However, after the injection of seawater and ten-times diluted seawater, the electrical conductivity decreases from λ_{max} towards λ_{min} and the reservoir wettability modifies towards water-wetting conditions. This lasts until $\lambda(x,t)$ reaches the value of λ_{min} where ω would become one. The relative permeability altered by the variation of electrical conductivity is presented by the following equation:

$$k_{rl}^{altered} = \omega k_{rl}^{water-wet} + (1-\omega) k_{rl}^{oil-wet},\quad \text{l = o, w}\ . \tag{21}$$

where $k_{rl}^{altered}$ is the altered relative permeability, and $k_{rl}^{water-wet}$ and $k_{rl}^{oil-wet}$are the water-wet and oil-wet relative permeabilities, respectively.

As the injection of engineered water reduces the electrical conductivity, it assists in shifting the wettability of the reservoir. The initial formation water relative permeability and altered wettability with the engineered water are depicted in **Fig. 30**. These relative permeability curves are obtained from Chandrasekhar and Mohanty (2013), where the effect of engineered water injection was investigated related to the formation damage caused by the injection of spiked sulfate and anhydrite precipitation. The results presented in the figure confirm that the injection of ten-times diluted seawater resulted in a more water-wet formation condition. Thus, with the injection of ten-times diluted seawater, the endpoint oil relative permeability increased from 0.123 to 0.5. This increase is quite distinct as compared to endpoint water relative permeability that decreased from 0.02 to 0.012. These results depict that the decrease in electrical conductivity actively altered the formation wettability towards water wetting conditions. These results are in agreement with Mahani *et al.* (2017) for the injection of engineered water and the increased recovery of oil from carbonates. The various parameters including residual water saturation, irreducible

oil saturation, Corey's exponents for oil and water, and endpoint for water and oil relative permeability curves are presented in **Table 6.**

The geochemical model based on the change in the formation electrical conductivity in this study is used to examine the injection of seawater and its dilution effects on oil recovery. We simulated three cases of water injection scenarios with different compositions. The various scenarios are Case 1 where formation water is injected with maximum electrical conductivity; Case 2 where seawater is injected with an electrical conductivity of 14.52 S/m, and Case 3 which represents the ten-times diluted seawater injection with the electrical conductivity of 2.96 S/m. It is important to mention here that the temperatures of the formation and engineered water were kept constant at 80 °C. The findings showed that the thickness of the electrical double layer increased with the injection of seawater and ten-times diluted seawater. The relative permeability curves and parameters at oil-wet (formation water) and water-wet conditions (engineered water) are depicted in **Fig. 30** and **Table 6,** respectively.

With the developed Matlab-IPhreeqc coupled simulator, we analyzed the influence of electrical conductivity variation during secondary and tertiary engineered water injection modes. The compositions of formation water, seawater- and different diluted-seawater can be found in **Table 6** and their order of injection is provided as follows:

a. Secondary Injection Mode: 1) Five (05) pore volumes of formation water, seawater and ten-times diluted seawater injection
b. Tertiary Injection Mode: 1) Two (02) pore volumes of formation water, 2) Three (03) pore volumes of seawater and ten-times diluted seawater injection

The accumulative recovery of oil with its profile during the injection of formation water, seawater, and ten-times diluted seawater in secondary and tertiary injection modes are presented in **Figs. 31** and **32,** respectively. **Fig. 31** which shows the secondary recovery reveals that the injection of ten-times diluted seawater (Case 3) resulted in a 52% oil recovery, which is the highest oil recovery as opposed to the injection of seawater (Case 2) and formation water (Case 3) which show 47% and 31% oil recoveries, respectively. Therefore, the injection of ten-times diluted seawater resulted in 21% and seawater in 16% additional oil as opposed to the injection of formation water. This is because the injection of formation water produced oil only due to the displacement without perturbing the equilibrium where the formation electrical conductivity remained the same. However, the injected seawater and ten-times diluted seawater decreased the formation electrical conductivity and succeeded in releasing bonded/trapped oil blobs. This decrease in electrical conductivity increases the EDL thickness and stabilized the water film. Therefore, the recovery of oil increases due to the significant decrease in the formation electrical conductivity. It is important to highlight that the injection of formation water follows the curves of oil-wet reservoir conditions with negligible wettability modification. These findings are further supported by the results depicted in **Figs. 25** and **28**, which show that wettability modification is more significant for ten-times diluted seawater injection (Case 3) as compared to the injection of seawater (Case 2). Thus, the injection of ten-times diluted seawater alters the formation wettability to more water-wet conditions due to the stabilization of the water film.

The oil recovery obtained during the injection of engineered water in tertiary flooding mode is presented in **Fig. 32**. The results of tertiary recovery are consistent with the findings of secondary injection. Thus, during the tertiary injection mode, the injection of ten-times diluted seawater results in the highest recovery of oil followed by seawater injection. This is because the injected formation water in the latter case is not successful in modifying the formation wettability and hence, the oil-wet state rests as before as it causes no variation in the electrical conductivity. This finding confirms that the engineered water injection was successful in decreasing the formation electrical conductivity. Thus, as per our findings, 21% of the oil production would be lost if formation water was injected instead of the proper water recipe (ten-times diluted seawater). Furthermore, a reduction in the ionic strength of water leads to a decrease in electrical conductivity and a substantial increase in the EDL thickness. Therefore, with the injection of engineered water (seawater/ modified seawater) the electrostatic force of repulsion

would increase leading to an increase in the water film thickness along with the rock-brine-oil interface. Thus, the rock is altered to a more water-wetting (hydrophilic) state with a significant increase in the oil recovery. Moreover, the injection of seawater would have resulted in an additional 16% oil as represented in **Figs. 31** and **32**. However, it is necessary to highlight that the injection of engineered water and the decrease in the formation electrical conductivity is a case-dependent phenomenon as it is controlled by the thermodynamic conditions, pore distributions, and crude oil/brine/rock interaction at a microscopic scale.

Conclusions

In this paper, the variation of formation electrical conductivity was investigated to determine the effect of its increase/decrease on oil recovery. We successfully determined the geochemical aspect of electrical conductivity by utilizing the developed Matlab-IPhreeqc coupled simulator. The important results and outcomes of this research are summarized below

- The developed geochemically coupled simulator can be used as an effective instrument to model the variation in the electrical conductivity and related oil recovery during engineered water injection.
- It was found that the temperature, ion mobility, and concentration of ionic species have a distinct impact on the formation electrical conductivity during engineered water injection. Ion mobility is an important parameter controlling the formation electrical conductivity for the investigated case study.
- The temperature of the injected water should be kept high in carbonates as this high temperature helps in increasing the electrical conductivity and the EDL thickness. The electrical conductivity and EDL thickness at 70°C were found to be 11.94 S/m and 0.317 nm. At 90°C electrical conductivity increased to 14.54 S/m, and EDL thickness to 0.319 nm. Finally, for 110°C the electrical conductivity increased to 17.12 S/m, and the EDL thickness to 0.321 nm.
- The injection of various water including seawater and its different dilution recipes decreases the electrical conductivity while the spiking of sulfate increases the ion mobility. The injection of seawater decreases the electrical conductivity from 35.28 S/m to 14.54 S/m. However, with the dilution of seawater, we observed a further decrease to 8.56, 2.95, 2.31, and 1.66 S/m for two-times diluted, 10-times diluted, 20-times diluted, and 100-times diluted, respectively.
- The concentration of sulfate during its spiking and dilution modified the formation electrical conductivity. However, the sulfate concentration should be optimized to increase the oil recovery and, avoid the formation, precipitation, and deposition of calcium sulfate.
- The variation of electrical conductivity by the injection of ten-times diluted seawater results in a significant increase in the oil recovery by approximately 21% for the presented case study.
- The variation in formation electrical conductivity by engineered water injection and the resulting oil recovery is a case-dependent phenomenon and should not be simply generalized.

Nomenclature

Symbols

a^0, b^0	=	Parameter for ion-size
A	=	Constant dependent on temperature
B	=	Constant dependent on temperature
E	=	Formation activation energy (J/mol)
H	=	Formation enthalpy (Joule)
I	=	Solution ionic strength

K	=	Geochemical reaction equilibrium constant
k	=	Permeability of reservoir (mD)
n	=	Concentration of ionic species (moles)
m	=	Molality of solution (mol/kgw)
P	=	formation pressure (psi)
q	=	Fluid flow rate (STB/Day)
R	=	Universal gas constant (J/mol.K)
S	=	Saturation of reservoir fluid (%)
T	=	Formation temperature (K)
V	=	Volume (m^3)
z	=	Charge of ionic species in formation fluid
Greek Letters		
μ	=	Viscosity of fluid (cP)
ρ	=	Density of fluid (kg/m^3)
ϕ	=	Porosity of rock (%)
ψ	=	Fractional flow function
λ	=	Fluid phase mobility
γ	=	Ion activity coefficient
ω	=	Interpolation parameter
Subscripts/Superscripts		
l	=	liquid
o	=	oil
w	=	water
Abbreviations		
EWI	=	Engineered Water Injection
PV	=	Pore Volume
TDS	=	Total Dissolved Solids

Acknowledgments

The authors wish to acknowledge Khalifa University of Science and Technology for funding this research. This publication is based upon work supported by the Khalifa University of Science and Technology under Award No. [8474000240]. We appreciate Emad W. Al Shalabi of the Petroleum Department, Khalifa University for fruitful discussion on engineered water injection.

References

1. Abdallah, W., Gmira, A., 2014. Wettability assessment and surface compositional analysis of aged calcite treated with dynamic water. *Energy & Fuels*, 28, 1652–1663, https://doi.org/10.1021/ef401908w.
2. Alotaibi, M.B., Yousef, A., 2017. The role of individual and combined ions in waterflooding carbonate reservoirs: electrokinetic study. *SPE Reservoir Evaluation and Engineering*, 20, 77–86.
3. Alotaibi, M. B., Cha, D., Alsofi, A. M., Yousef, A. A., 2018. Dynamic interactions of inorganic species at carbonate/brine interfaces: an electrokinetic study. *Colloids and Surfaces A: Physicochemical and Engineering Aspects*, 550, 222–235, https://doi.org/10.1016/j.colsurfa.2018.04.042.
4. Al-Shalabi, E. W., Sepehrnoori, K., and Pope, G., 2015. Geochemical Interpretation of Low-Salinity-Water Injection in Carbonate Oil Reservoirs. *SPE Journal*, 20 (06): 1212 – 1226.
5. Al-Shalabi, E. W. and Sepehrnoori, K., 2017. *Low Salinity and Engineered Water Injection for Sandstone and Carbonate Reservoirs*. Gulf Professional Publishing, Elsevier, 1st Edition, pp. 178, ISBN: 978-0-12-813604-1, Cambridge, USA.

6. Austad, T., Shariatpanahi, S. F., Strand, S., Aksulu, H., Puntervold, T., 2015. Low salinity EOR effects in limestone reservoir cores containing anhydrite: a discussion of the chemical mechanism. *Energy & Fuels*, 29, 6903–6911, https://doi.org/10.1021/acs.energyfuels.5b01099.
7. Bear, J., 2013. *Dynamics of Fluids in Porous Media*. Courier Dover Publications.
8. Boampong, L. O., Rafati, R., & Haddad, A. S., 2022. A calibrated surface complexation model for carbonate-oil-brine interactions coupled with reservoir simulation-Application to controlled salinity water flooding. *Journal of Petroleum Science and Engineering*, 208, 109314.
9. Brady, P. V., Thyne, G., 2016. Functional wettability in carbonate reservoirs. *Energy & Fuels*, 30, 9217–9225, https://doi.org/10.1021/acs.energyfuels.6b01895.
10. Chandrasekhar, S. and Mohanty, K. K., 2013. Wettability Alteration with Brine Composition in High-Temperature Carbonate Reservoirs. Paper SPE 166280, *SPE Annual Technical Conference and Exhibition*, New Orleans, Louisiana, USA.
11. Chandrasekhar, S., Sharma, H., Mohanty, K. K., 2018. Dependence of wettability on brine composition in high temperature carbonate rocks. *Fuel* 225, 573–587, https://doi.org/10.1016/j.fuel.2018.03.176.
12. Chen, Y., Xie, Q., Sari, A., Brady, P.V., Saeedi, A., 2018. Oil/water/rock wettability: influencing factors and implications for low salinity water flooding in carbonate reservoirs. *Fuel*, 215,171–177, https://doi.org/10.1016/j.fuel.2017.10.031.
13. De Bruin, W. J., 2012. *Simulation of Geochemical Processes during Low Salinity Water Flooding by Coupling Multiphase Buckley-Leverett Flow to the Geochemical Package PHREEQC*. MS Thesis. The Delft University of Technology. Delft, The Netherland.
14. Dukhin, A. S., Goetz, P. J., 2012. Colloidal systems - Methods for zeta-potential determination-Part 1: Electroacoustic and electrokinetic phenomena. *International Standard ISO 13099*. https://www.iso.org/standard/52807.html.
15. Ejeh, C., Afgan, I., AlMansob, H., Brantson, E., Fekala, J., Odiator, M., Stanley, P., Anumah, P., Onyekperem, C., Boah, E., 2020. Computational fluid dynamics for ameliorating oil recovery using silicon-based nanofluids and ethanol in oil-wet reservoirs. *Energy Reports*, 6, 3023-3035.
16. Fathi, S. J., Austad, T., Strand, S., 2011. Water-based enhanced oil recovery (EOR) by "Smart Water": optimal ionic composition for EOR in carbonates. *Energy Fuels*, 25 (11), 5173–5179.
17. Farajzadeh, R., Matsuura, T., van Batenburg, D., and Dijk, H., 2012. Detailed Modeling of the Alkali/Surfactant/Polymer (ASP) Process by Coupling a Multipurpose Reservoir Simulator to the Chemistry Package PHREEQC. *SPE Reservoir Evaluation & Engineering*. 15(4): 423-435. SPE-143671-PA. http://dx.doi.org/10.2118/143671-PA.
18. Hiorth, A., Cathles, L.M., Madland, M.V., 2010. The Impact of Pore Water Chemistry on Carbonate Surface Charge and Oil Wettability. *Transport in Porous Media*, 85: 1–21, https://doi.org/10.1007/s11242-010-9543-6.
19. Jerauld, G. R., Webb, K. J., Lin, C.Y., and Seccombe, J. C., 2008. Modeling Low-Salinity Waterflooding. *SPE Reservoir Evaluation & Engineering*, 11(6): 1000-1012.
20. Kasha, A., Al-Hashim, H., Abdallah, W., Taherian, R., Sauerer, B., 2015. Effect of Ca^{2+}, Mg^{2+}, and SO_4^{2-} ions on the zeta potential of calcite and dolomite particles aged with stearic acid. *Colloids and Surfaces A: Physicochemical and Engineering Aspects*, 482, 290–299, https://doi.org/10.1016/j.colsurfa.2015.05.043.
21. Khormali, A., Petrokov, D. G., and Moein, M. J. A., 2016. Experimental Analysis of Calcium Carbonate Scale Formation and Inhibition in Waterflooding of Carbonate Reservoirs. *Journal of Petroleum Science and Engineering*, 147: 843-850.
22. Khurshid, I., Al-Shalabi, E. W., and Afgan, I., 2022a. New Insights into Surfactant Adsorption Estimation in Carbonates under Harsh Conditions Using Surface Complexation Modeling. *SPE Reservoir Evaluation & Engineering-Reservoir Engineering*. SPE-207912-PA.
23. Khurshid, I., Al-Shalabi, E. W., Afgan, I., and Al-Attar, H., 2022b. A Numerical Approach to Investigate the Impact of Acid-Asphaltene Sludge Formation on Wormholing during Carbonate Acidizing. *Journal of Energy Resources Technology*, 144 (6):063001. https://doi.org/10.1115/1.4051738.
24. Khurshid, I., Al-Shalabi., 2022. New Insights into Modeling Disjoining Pressure and Wettability Alteration by Engineered Water: Surface Complexation based Rock Composition Study. *Journal of Petroleum Science and Engineering*, 208, 10984.

25. Khurshid, I., and Afgan, I., 2021a. Investigation of Water Composition on Formation Damage and Related Energy Recovery from Geothermal Reservoirs: Geochemical and Geomechanics Insights. *Energies*, 14 (21): 7415.
26. Khurshid, I., and Afgan, I, 2021b. Geochemical Investigation of CO_2 Injection in Oil and Gas Reservoirs of Middle East to Estimate the Formation Damage and Related Oil Recovery. *Energies*, 14 (22): 7676.
27. Khurshid, I., and Fujii, Y., 2021. Geomechanical analysis of formation deformation and permeability enhancement due to low-temperature CO_2 injection in subsurface oil reservoirs. *Journal of Petroleum Exploration and Production Technology*, 11(4): 1915:1923.
28. Khurshid, I., Al-Shalabi, E. W., and Alameri, W., 2020. Influence of Water Composition on Formation Damage and Related Oil Recovery in Carbonates: A Geochemical Study. *Journal of Petroleum Science and Engineering*, 107715, 195: 1-21.
29. Khurshid, I., Al-Shalabi, E. W., Al-Attar, H, and Alneaimi, A., 2020. Analysis of Fracture Choking due to Asphaltene Deposition in Fractured reservoirs and its Effect on Productivity. *Journal of Petroleum Exploration and Production Technology*, 10: 3377-3387.
30. Khurshid, I., Al-Attar, H., Alraeesi, A. R., 2018. Modeling Cementation in Porous Media during Waterflooding: Asphaltene deposition, Formation dissolution and their Cementation. *Journal of Petroleum Science and Engineering*, 161: 359-367.
31. Khurshid, I., and Choe, J., 2016. Analysis of Carbon dioxide Temperature, its thermal disturbance and evaluating the formation damages during its injection in shallow, deep and high temperature reservoirs. *International Journal of Oil, Gas and Coal Technology*, 11(2): 141-153.
32. Khurshid, I., Fujii, Y., and Choe, J., 2015. Analytical Model to Determine CO_2 Injection Time in a Reservoir for Optimizing its Storage and Oil Recovery: A Reservoir Compaction Approach. *Journal of Petroleum Science and Engineering*, 135: 240-245.
33. Khurshid, I., and Choe, J., 2015. Analysis of Asphaltene Deposition, Carbonate Precipitation, and their Cementation in Depleted Reservoirs during CO_2 Injection. *Greenhouse Gases: Science and Technology*, 5(5): 657-667.
34. Korrani, A. K. N., 2014. *Mechanistic Modeling of Low Salinity Water Injection*. Ph.D. dissertation, the University of Texas at Austin, Austin, Texas, USA.
35. Korrani, A.K.N., Jerauld, G.R., Sepehrnoori, K., 2016. Mechanistic Modeling of Lowsalinity Waterflooding through Coupling a Geochemical Package with a Compositional Reservoir Simulator. *SPE Reservoir Evaluation & Engineering*, 19 (01): 142-162.
36. Korrani, A. K. N., and Jerauld G. R., 2019. Modeling Wettability Change in Sandstones and Carbonates using a Surface-Complexation-Based Method. *Journal of Petroleum Sciences and Engineering*, 174: 1093-1112.
37. Ligthelm, D. J., Gronsveld, J., Hofman, J., Brussee, N., Marcelis, F., and van der Linde, H., 2009. Novel Waterflooding Strategy by Manipulation of Injection Brine Composition. Paper SPE 119835, *EUROPEC/EAGE Conference and Exhibition*, Amsterdam, Netherlands.
38. Mahani, H., Sorop, T., Ligthelm, D.J., Brooks, D., Vledder, P., Mozahem, F., Ali, Y., 2011. Analysis of field responses to low-salinity waterflooding in secondary and tertiary mode in Syria, *SPE EUROPEC/EAGE Annual Conference and Exhibition*, Society of Petroleum Engineers.
39. Mahani, H., Keya, A.L., Berg, S., Bartels, W.B., Nasralla, R., Rossen, W.R., 2015. Insights into the mechanism of wettability alteration by low-salinity flooding (LSF) in carbonates. *Energy & Fuels* 29. https://doi.org/10.1021/ef5023847.
40. Mahani, H., Keya, A.L., Berg, S., Nasralla, R., 2017. Electrokinetics of carbonate/brine interface in low-salinity waterflooding: effect of brine salinity, composition, rock type, and pH on zeta-potential and a surface-complexation model. *SPE Journal*, 22, 053–068, https://doi.org/10.2118/181745-PA.
41. Nasralla, R.A., Sergienko, E., Masalmeh, S.K., van der Linde, H.A., Brussee, N.J., Mahani, H., Suijkerbuijk, B.M.J.M., and Al-Qarshubi, I.S.M., 2016. Potential of low-salinity waterflood to improve oil recovery in carbonates: demonstrating the effect by qualitative coreflood. *SPE Journal*, 21, 1643–1654, https://doi.org/10.2118/172010-PA.
42. Ouden, L. D., 2014. *Calcite Dissolution Behaviour during Low Salinity Water Flooding in Carbonate Rock.* Delft University of Technology, 2014. http://repository.tudelft.nl/view/ir/uuid:8be82b5f-7945-4eef-953f-248ef2d6b16a/.

43. Parkhurst, D. L., and Appelo, C. A. J., 2013. *Description of Input and Examples for PHREEQC Version 3–A Computer Program for Speciation, Batch-reaction, One-dimensional Transport, and Inverse Geochemical Calculations.* In US Geological Survey Techniques and Methods, Section A: Groundwater, Book 6: Modeling Techniques, Chap. 43. Denver: US Geological Survey.
44. Purswani, P., Karpyn, Z.T., 2019. Laboratory investigation of chemical mechanisms driving oil recovery from oil-wet carbonate rocks. *Fuel*, 235, 406–415, https://doi.org/10.1016/j.fuel.2018.07.078.
45. Qiao, C., Li, L., Johns, R.T., Xu, J., 2015. A Mechanistic Model for Wettability Alteration by Chemically Tuned Waterflooding in Carbonate Reservoirs. *SPE Journal*. https://doi.org/10.2118/170966-PA.
46. Sari, A., Chen, Y., Xie, Q., Saeedi, A., 2019. Low salinity water flooding in high acidic oil reservoirs: impact of pH on wettability of carbonate reservoirs. *Journal of Molecular Liquid*, 281, 444–450, https://doi.org/10.1016/j.molliq.2019.02.081.
47. Seccombe, J., Lager, A., Jerauld, G., Jhaveri, B., Buikema, T., Bassler, S., Denis, J., Webb, K., Cockin, A., Fueg, E., 2010. Demonstration of low-salinity EOR at Interwell Scale, Endicott Field, Alaska, *SPE Improved Oil Recovery Symposium*, Society of Petroleum Engineers.
48. Strand, S., Standnes, D. C., and Austad, T., 2006. New Wettability Test for Chalk based on Chromatographic Separation of SCN^- and SO_4^{2-}. *Journal of Petroleum Science and Engineering*, 52(1): 187–197.
49. Sanaei, A., Tavassoli, S., and Sepehrnoori, K., 2018. Investigation of Modified Water Chemistry for Improved Oil Recovery: Application of DLVO Theory and Surface Complexation Model. Paper SPE 190017, *SPE Western Regional Meeting*, California, USA.
50. Taheriotaghsara, M., Eftekhari, A. A., Nick, H., M., 2020. Adsorption- and Diffusion-Controlled Wettability Change in Modified Salinity Water Flooding. *Energy & Fuels*, 34, 13767-13781.
51. Tetteh, J.T., Pham, A., Peltier, E., Hutchison, J.M., Ghahfarokhi, R.B., 2022. Predicting the electrokinetic properties on an outcrop and reservoir composite carbonate surfaces in modified salinity brines using extended surface complexation models. *Fuel*, 309, 122078.
52. Udoh, T., and Vinogradov, J., 2019. Effects of Temperature on Crude-Oil-Rock-Brine Interaction during Controlled Salinity Biosurfactant Flooding. Paper SPE 198761, *Nigeria Annual International Conference and Exhibition*, Lagos, Nigeria.
53. Wei, L. 2012. Sequential Coupling of Geochemical Reactions with Reservoir Simulations for Waterflood and EOR Studies. *SPE Journal*. 17(2): 469-484. SPE-138037-PA. http://dx.doi.org/10.2118/138037-PA.
54. Xie, Q., Sari, A., Pu, W., Chen, Y., Brady, P.V., Al Maskari, N., Saeedi A., 2018. pH effect on wettability of oil/brine/carbonate system: implications for low salinity water flooding. *Journal of Petroleum Science and Engineering*, 168, 419–425, https://doi.org/10.1016/j.petrol.2018.05.015.
55. Xie, Q., Liu, Y., Wu, J., and Liu, Q., 2014. Ions Tuning Water Flooding Experiments and Interpretation by Thermodynamics of Wettability. *Journal of Petroleum Science and Engineering*, 124: 350-358.
56. Yousef, A.A., Al-Saleh, S.H., Al-Kaabi, A., Al-Jawfi, M.S., 2011. Laboratory investigation of the impact of injection-water salinity and ionic content on oil recovery from carbonate reservoirs. *SPE Reservoir Evaluation and Engineering*, 14, 578–593, https://doi.org/10.2118/137634-PA.
57. Zhang, P., Tweheyo, M. T., and Austad, T., 2007. Wettability Alteration and Improved Oil Recovery by Spontaneous Imbibition of Seawater into Chalk: Impact of the Potential Determining ions Ca^{2+}, Mg^{2+}, and SO_4^{2-}. *Colloids and surfaces A: Physicochemical and Engineering Aspects*, 301(1): 199–208.

Table 1: Formation water and injected seawater composition used for scale precipitation modeling

Salinity Unit	ppm								meq/ml	
Ions	**Ca^{+2}**	**Na^{+}**	**Cl^{-}**	**SO_4^{-2}**	**Mg^{+2}**	**HCO_3^{-1}**	**K^{+}**	**TDS**	**Anions**	**Cations**
Field Formation Water	2,043	42,367	71,200	108	574	1,615	1,759	119,666	2.03	2.00
Original Seawater	323	11,002	20,138	2,479	1,425	74	348	35,789	0.62	0.60

Table 2: Details of carbonates composition, core lithology, elements, and grid block details used in the simulation runs for scale precipitation modeling

Lithology (%)	Calcite (81), Dolomite (12), Clay (7)
Elements	Calcium, Sodium, Potassium, Chloride, Magnesium, Bicarbonate, Sulfate
Core Model Dimensions (m)	0.0355 × 0.0293 × 0.0293 (Length, Width, and Height)
Number of Grid blocks	20 × 1 × 1 (1D Model)
Grid block Sizes	0.001775 × 0.0293 × 0.0293 (Δx, Δy, and Δz)
Shifts	45
Time-step	216
Flow direction	Forward
Boundary conditions	Flux-flux
Diffusion coefficient	0.3×10-9
Dispersivity	0.0005
Porosity (%)	17.3
Permeability (mD)	26.1
Core Length (cm)	3.55
Core Diameter (cm)	2.93
Temperature (°C)	80

Table 3: Compositions of waters used for the validation of electrical conductivity

Salinity Unit	mol/L						ppm	meq/ml	
Ionic Species	**Ca^{+2}**	**Na^{+}**	**Cl^{-}**	**SO_4^{-2}**	**Mg^{+2}**	**K^{+}**	**TDS**	**Anions**	**Cations**
Formation Water	0.42	1.46	2.49	0.004	0.09	0	141149	2.49	2.49
Engineered Water	1.56×10^{-4}	6.1×10^{-3}	6.9×10^{-3}	2.65×10^{-4}	5.0×10^{-4}	0	429	0.01	0.01

Table 4: Details of carbonate lithology, various elements, and grid details used for electrical conductivity modeling

Formation Lithology (%)	Anhydrite (1), Calcite (95), Dolomite (4)
Elements in formation	Calcium, Chloride, Magnesium, Potassium, Sodium, Sulfate
Grid blocks dimension	20 × 1 × 1 (1D Model)
Shifts	800
Time-step	50
Flow direction	Forward
Boundary conditions	Flux-flux
Diffusion coefficient	0.3×10^{-9}
Dispersivity	0.0005
Thermal diffusion coefficient	0.5×10^{-6}
Temperature retardation factor	3
Formation porosity (%)	28
Formation permeability (mD)	127
Length of core (cm)	7.62
Diameter of core (cm)	3.78
Formation temperature (°C)	70

Table 5: Detail ionic compositions of various waters used in the sensitivity analysis

Salinity Unit			**mol/L**						**ppm**	**meq/ml**	
Ionic composition			**Ca^{+2}**	**Na^{+}**	**Cl^{-}**	**SO_4^{-2}**	**Mg^{+2}**	**K^{+}**	**TDS**	**Anions**	**Cations**
Formation Water			0.42	1.46	2.49	0.004	0.09	0	141149	2.49	2.49
Seawater			0.014	0.55	0.62	0.024	0.045	0	38580	0.67	0.67
Modified Seawater	**Sulfate content**	**Two-Times Spiked Sulfate**	0.014	0.5505	0.555	0.048	0.045	0	38580	0.60	0.60
		Two-Times Diluted Sulfate	0.014	0.584	0.63	0.012	0.045	0	38580	0.64	0.64
		Four-Times Diluted Sulfate	0.014	0.591	0.642	0.006	0.045	0	38580	0.65	0.65
		Two-Times Diluted	0.007	0.275	0.31	0.012	0.0225	0	19290	0.33	0.33

	Water dilution	**10-Times Diluted**	0.0014	0.05	0.062	0.0024	0.0045	0	3858	0.07	0.07
		20-Times Diluted	0.0007	0.0275	0.031	0.0012	0.00225	0	1929	0.03	0.03
		100-Times Diluted	0.00014	0.005	0.0062	0.00024	0.00045	0	386	0.01	0.01

Table 6: Relative permeability data for oil recovery due to variation in electrical conductivity

Parameters		**Values**
Viscosity of Water (cP)		1
Viscosity of Oil (cP)		2
Water Saturation: Irreducible (S_{wirr})		0.200
Initial (Oil-wet) Relative Permeability Parameters	**Corey's Exponent: Water (n_w)**	2.55
	Corey's Exponent: Oil (n_o)	3.03
	Oil Saturation: Residual (S_{or})	0.470
	Oil Relative Permeability: Endpoint (k_{ro})	0.123
	Water Relative Permeability: Endpoint (k_{rw})	0.020
Final (Water-wet) Relative Permeability Parameters	**Corey's Exponent: Water (n_w)**	2.60
	Corey's Exponent: Oil (n_o)	2.80
	Oil Saturation: Residual (S_{or})	0.163
	Oil Relative Permeability: Endpoint (k_{ro})	0.500
	Water Relative Permeability: Endpoint (k_{rw})	0.012

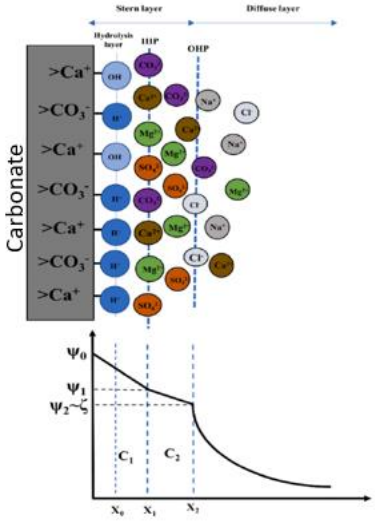

Fig. 1: Electrical double layer configuration in the porous media (Tetteh *et al.*, 2022**).**

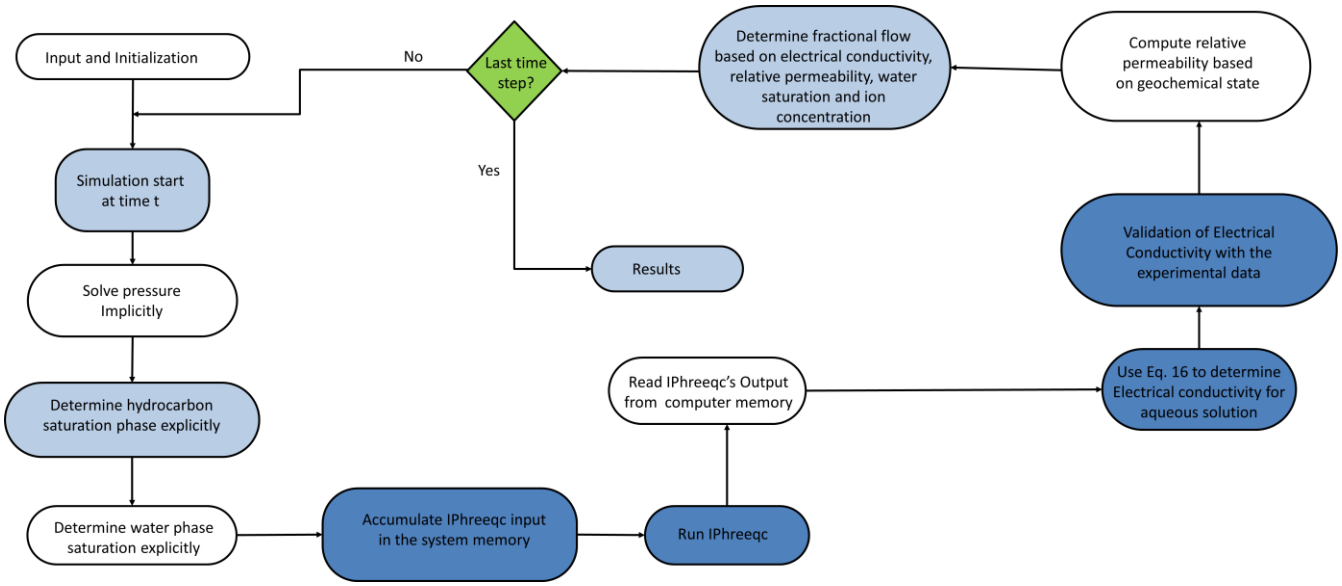

Fig. 2: Flowchart of Matlab and IPhreeqc coupled simulator

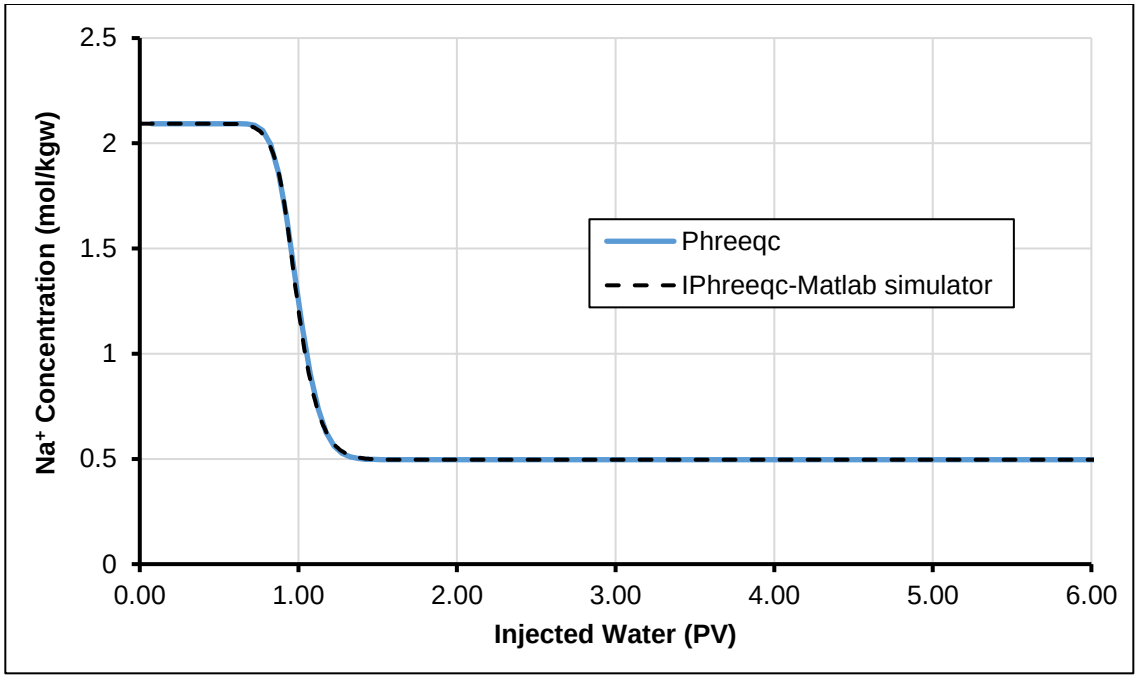

Fig. 3: Comparison of sodium ion concentration with Phreeqc and IPhreeqc coupled simulator.

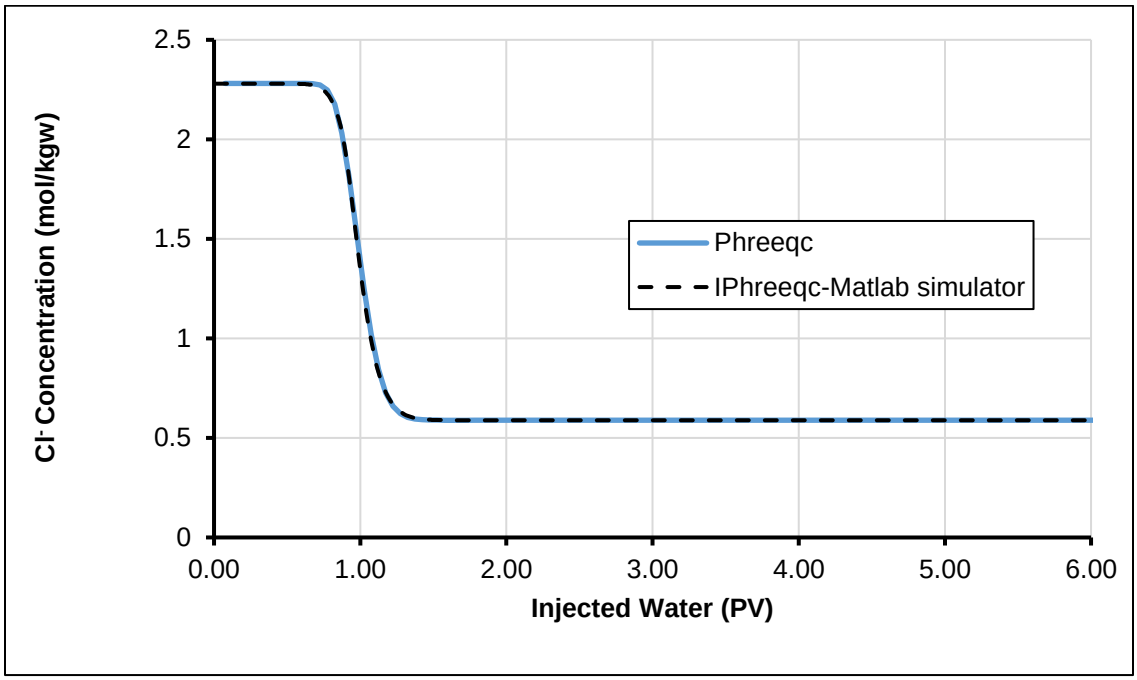

Fig. 4: Comparison of chloride ion concentration with Phreeqc and IPhreeqc coupled simulator.

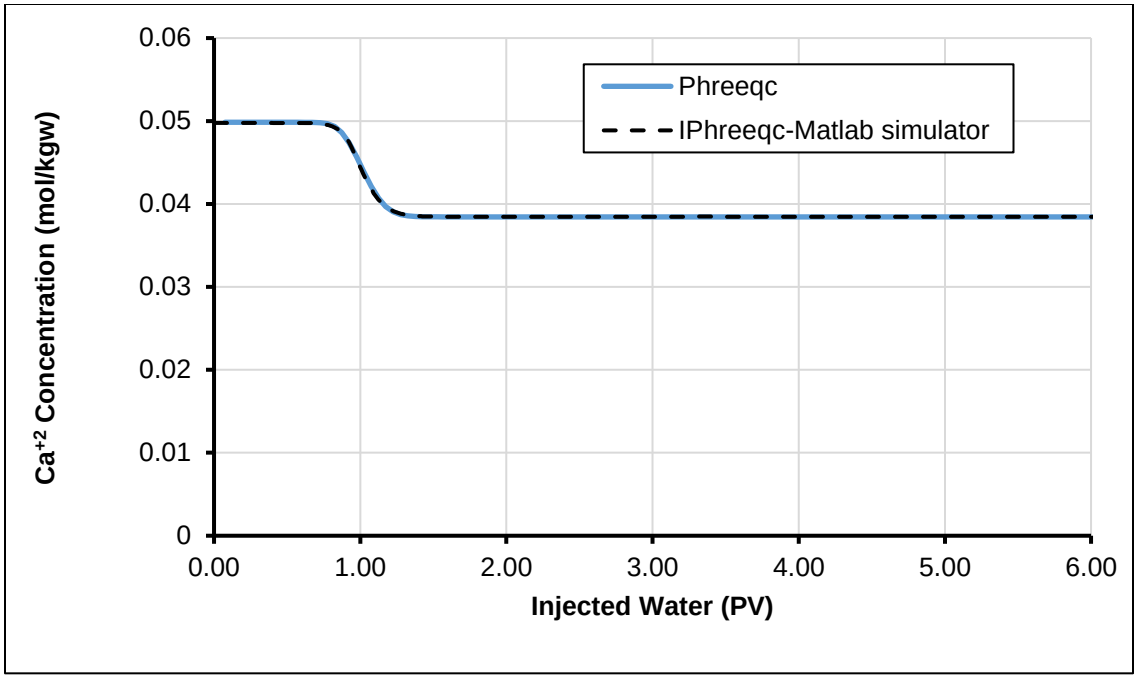

Fig. 5: Comparison of calcium ion concentration with Phreeqc and IPhreeqc coupled simulator.

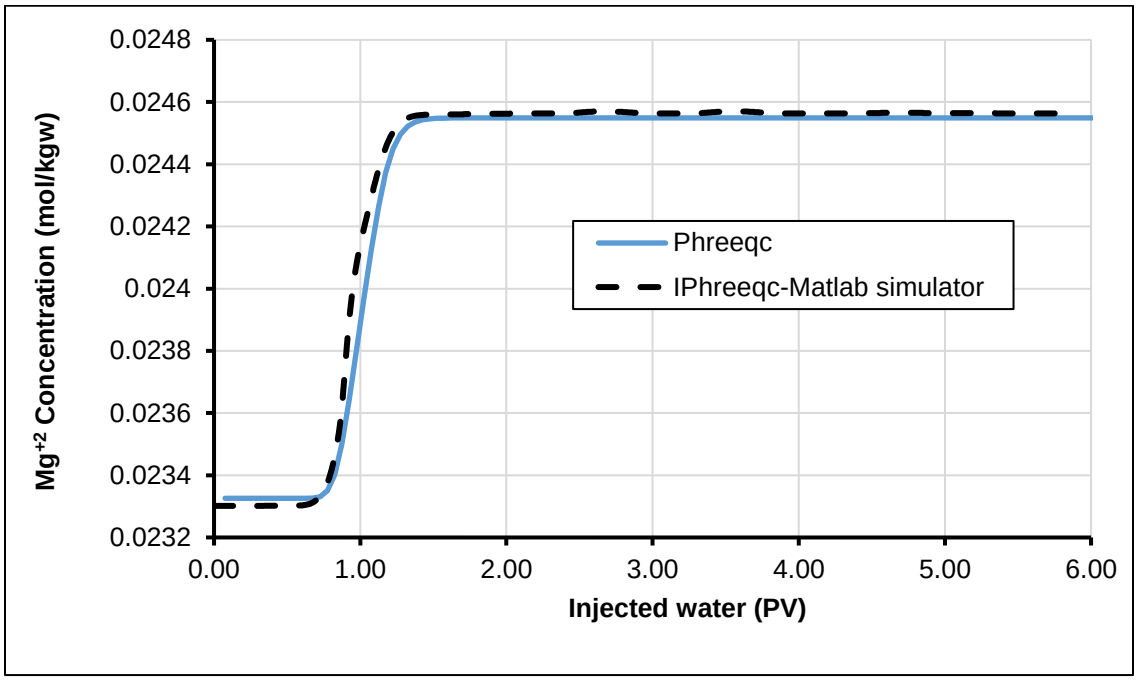

Fig. 6: Comparison of magnesium ion concentration with Phreeqc and IPhreeqc coupled simulator.

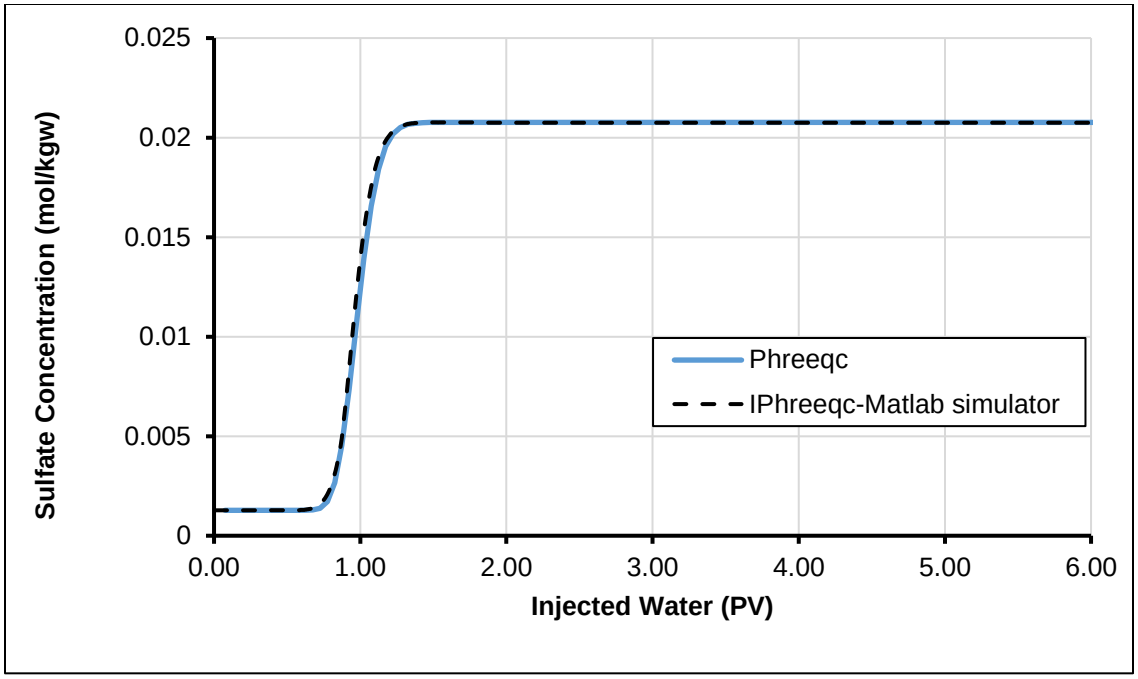

Fig. 7: Comparison of sulfate ion concentration with Phreeqc and IPhreeqc coupled simulator.

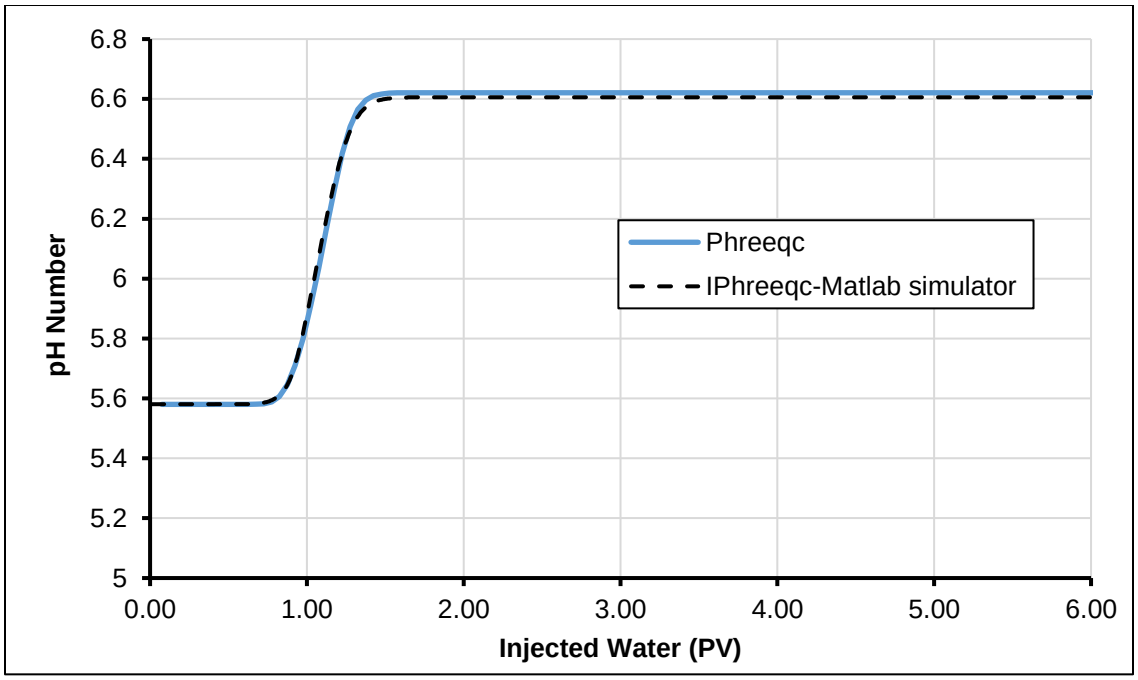

Fig. 8: Comparison of pH Number with Phreeqc and IPhreeqc coupled simulator.

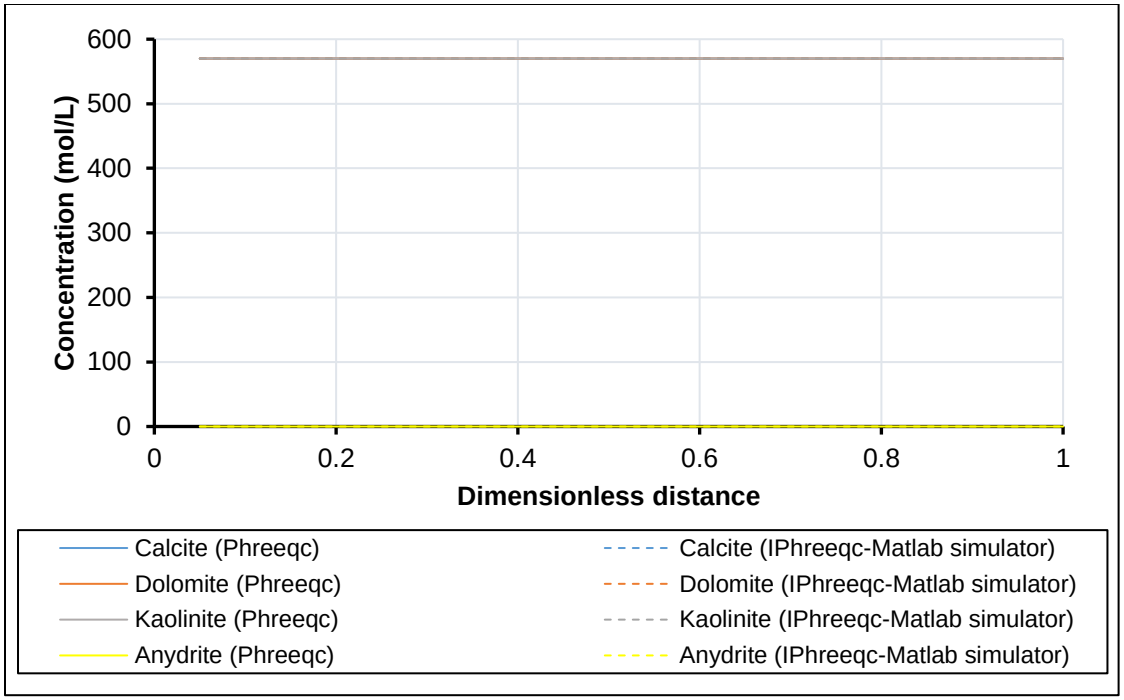

Fig. 9: Comparison of initial concentration of solid species at 0 PV of injected seawater with Phreeqc and IPhreeqc coupled simulator.

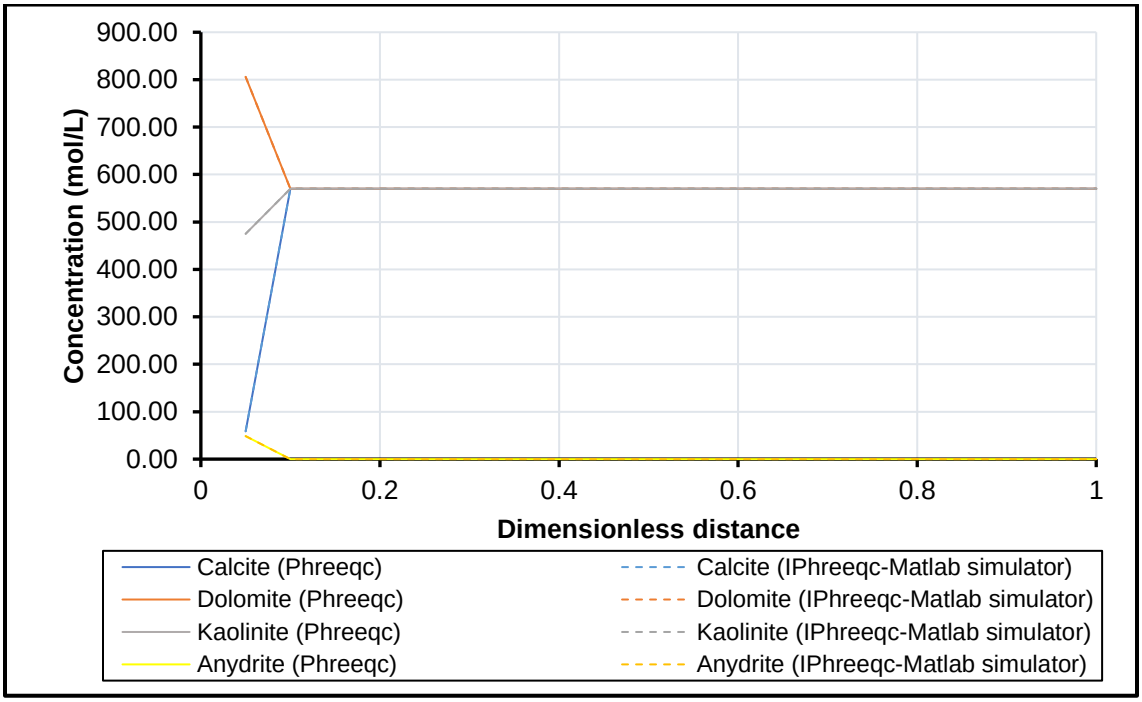

Fig. 10: Comparison of the final concentration of solid species at 6 PV of injected seawater with Phreeqc and IPhreeqc coupled simulator.

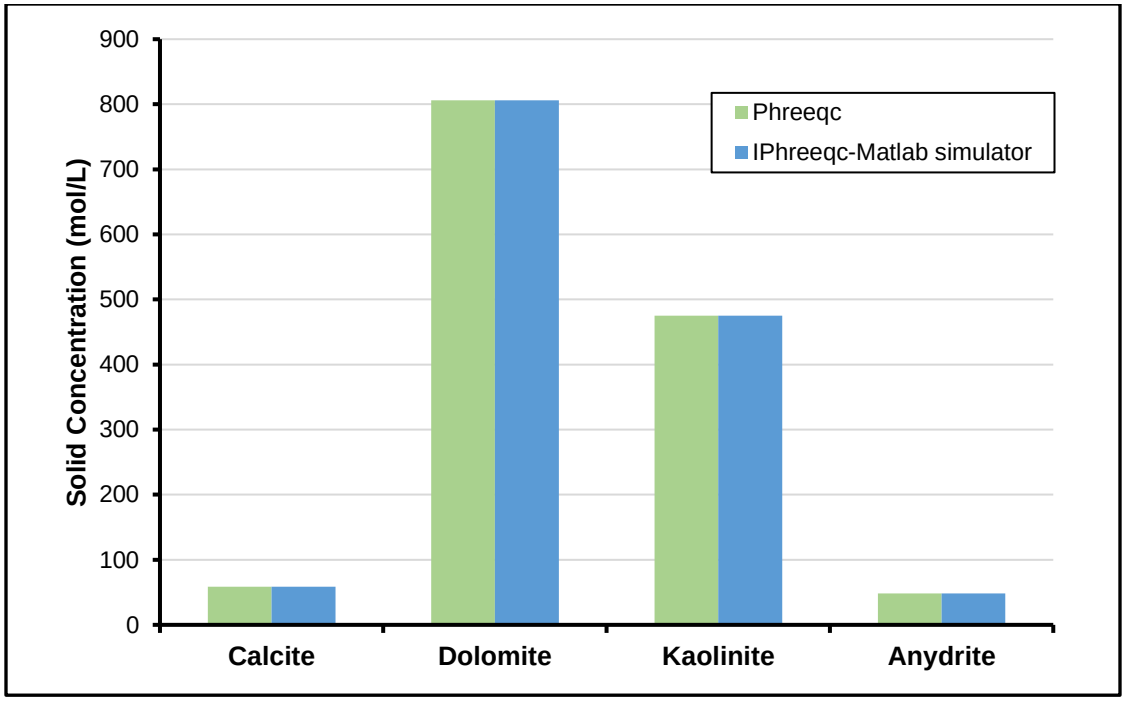

Fig. 11: Comparison of solid species concentration at 6 PV of injected seawater with Phreeqc and IPhreeqc coupled simulator.

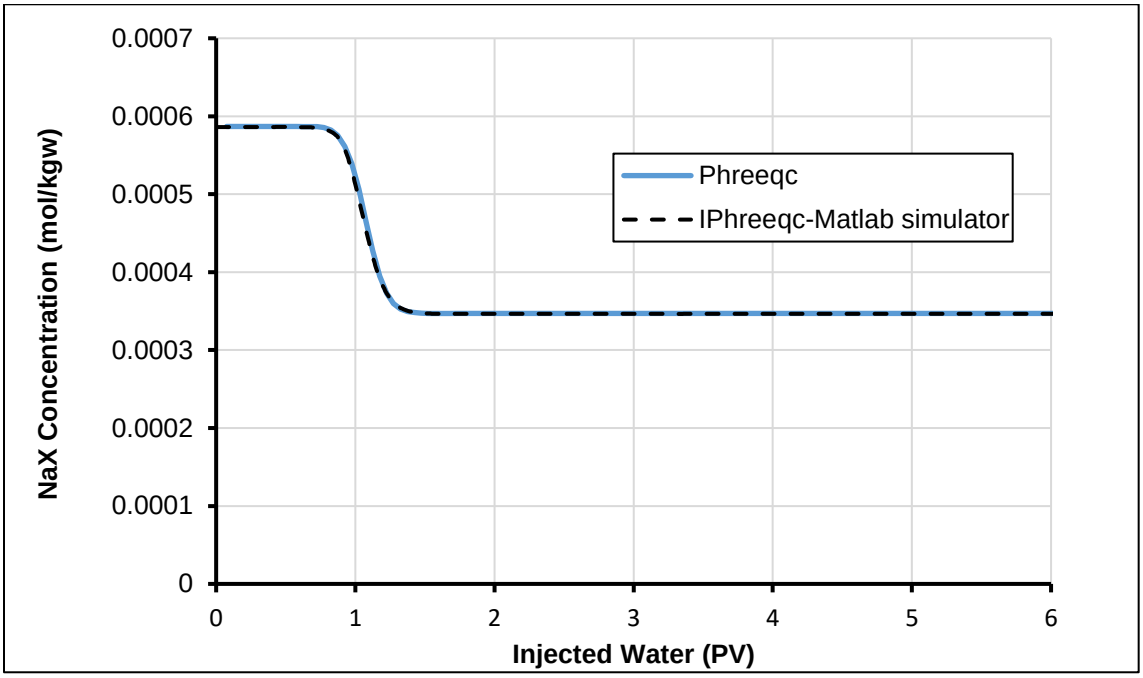

Fig. 12: Comparison of NaX concentration with Phreeqc and IPhreeqc coupled simulator.

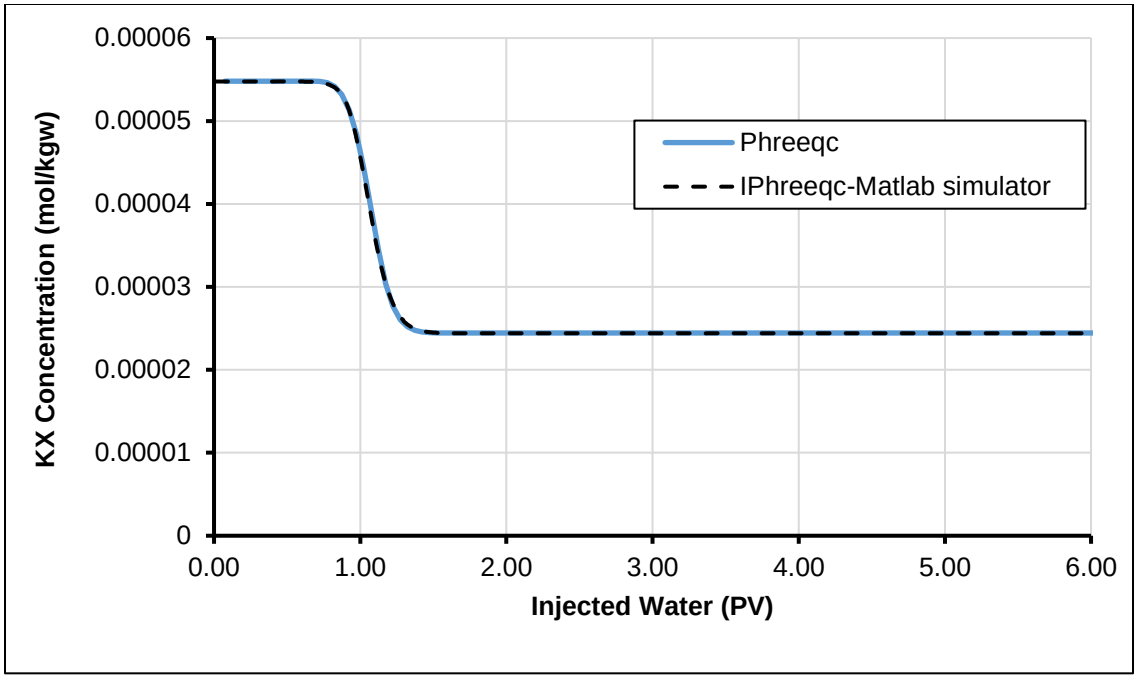

Fig. 13: Comparison of KX concentration with Phreeqc and IPhreeqc coupled simulator.

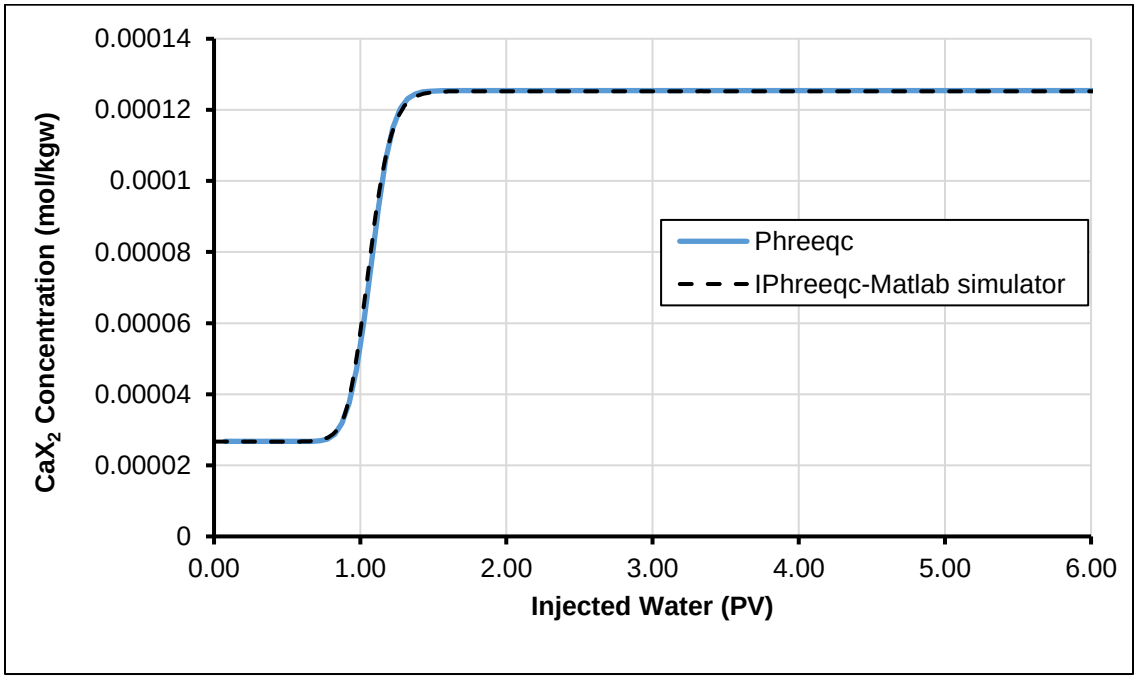

Fig. 14: Comparison of CaX_2 concentration with Phreeqc and IPhreeqc coupled simulator.

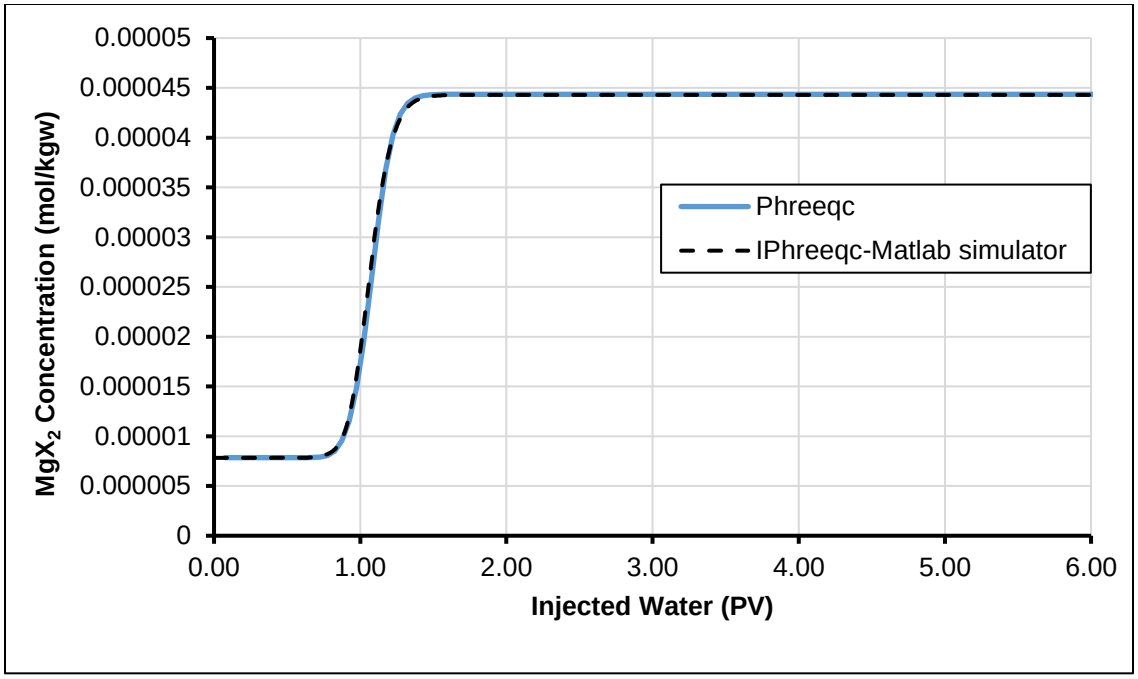

Fig. 15: Comparison of MgX_2 concentration with Phreeqc and IPhreeqc coupled simulator.

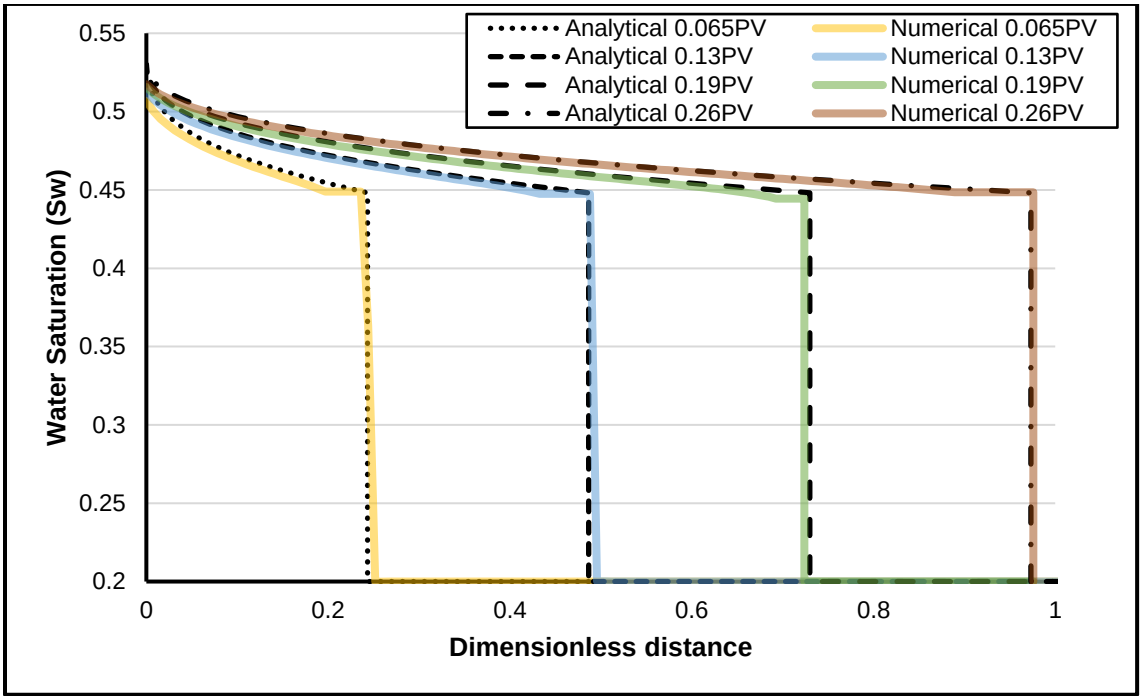

Fig. 16: Comparison of the numerical solution by the developed model with Buckley-Leverette displacement equation.

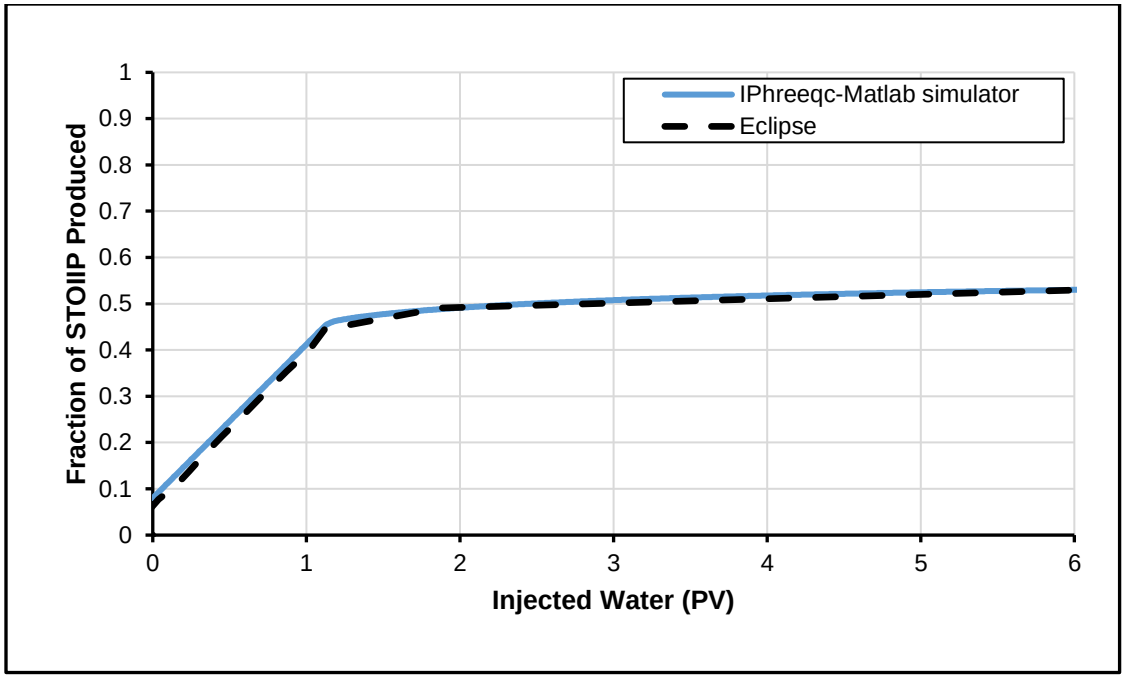

Fig. 17: Comparison of numerical solution of the developed model with the commercial simulator.

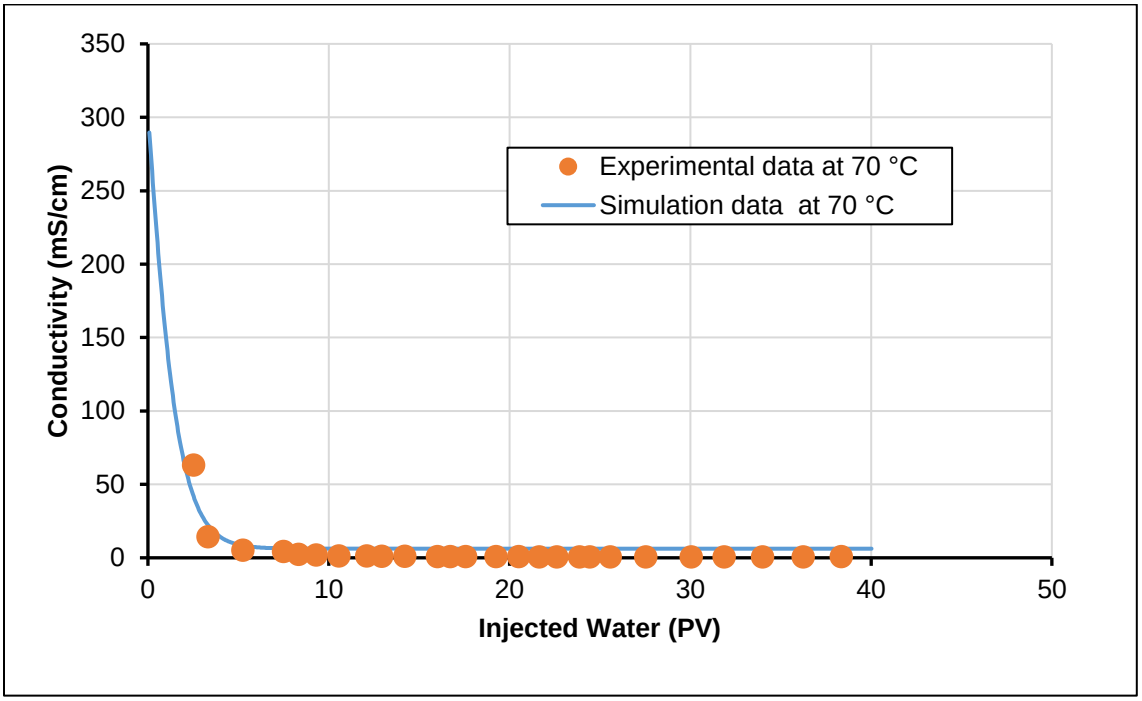

Fig. 18: Comparison of electrical conductivity simulation data and experimental data (Udoh and Vinogradov, 2019).

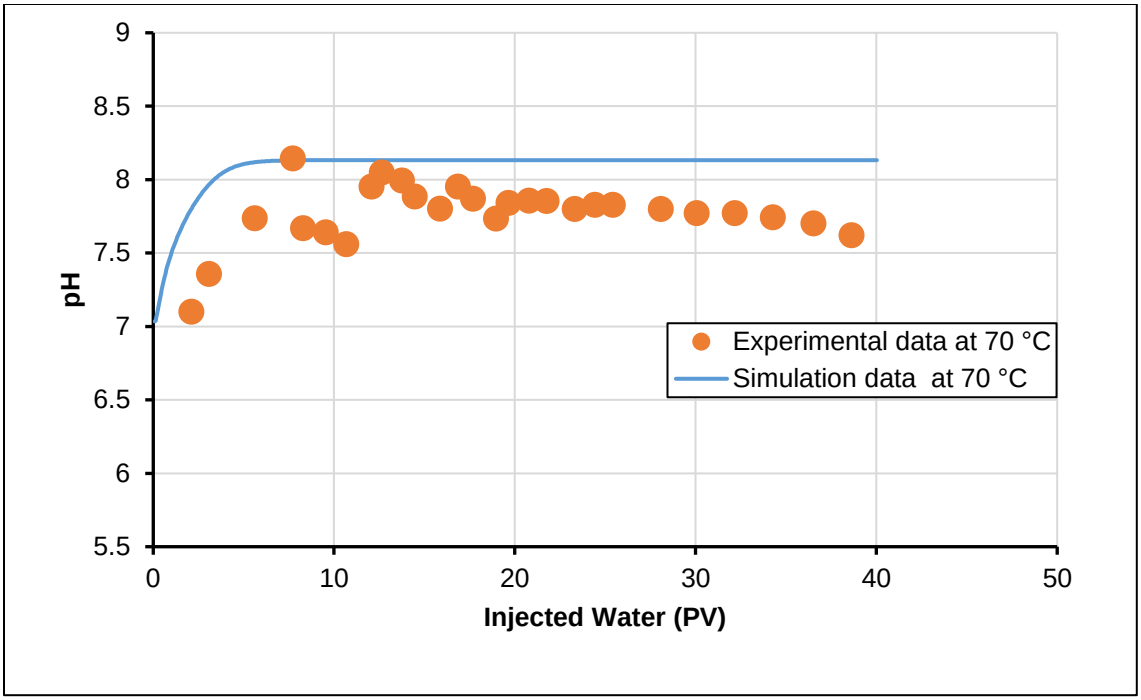

Fig. 19: Comparison of pH simulation data and experimental data (Udoh and Vinogradov, 2019).

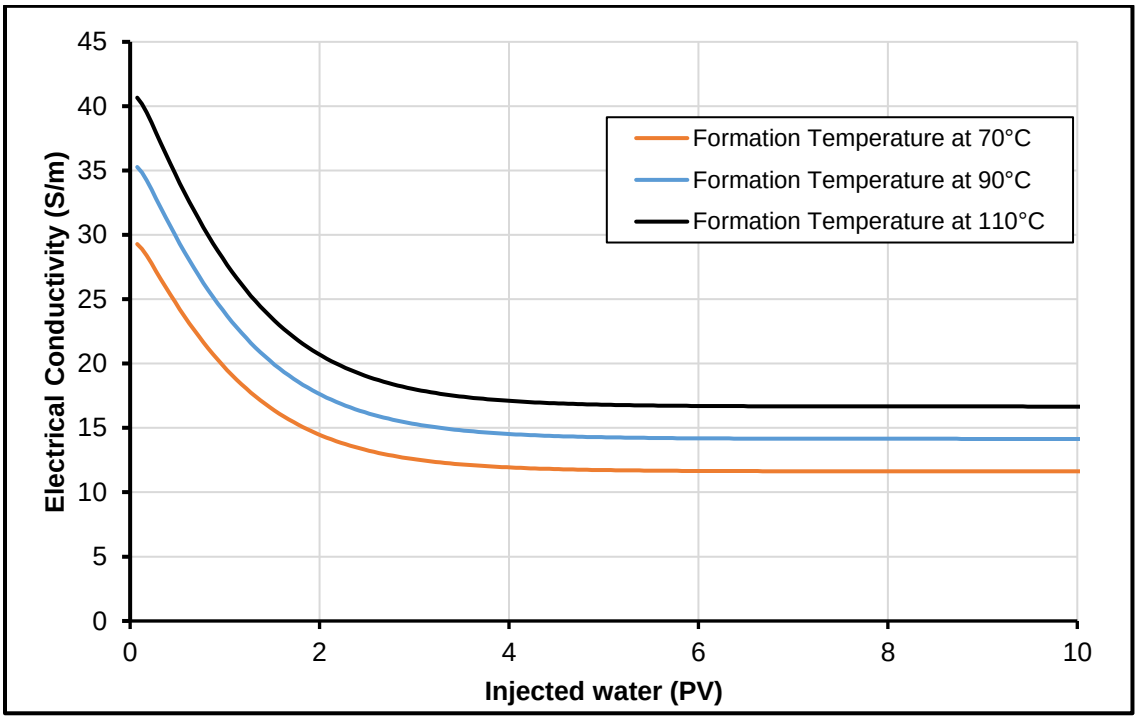

Fig. 20: Variation of electrical conductivity due to temperature change during seawater injection for 10 PVs.

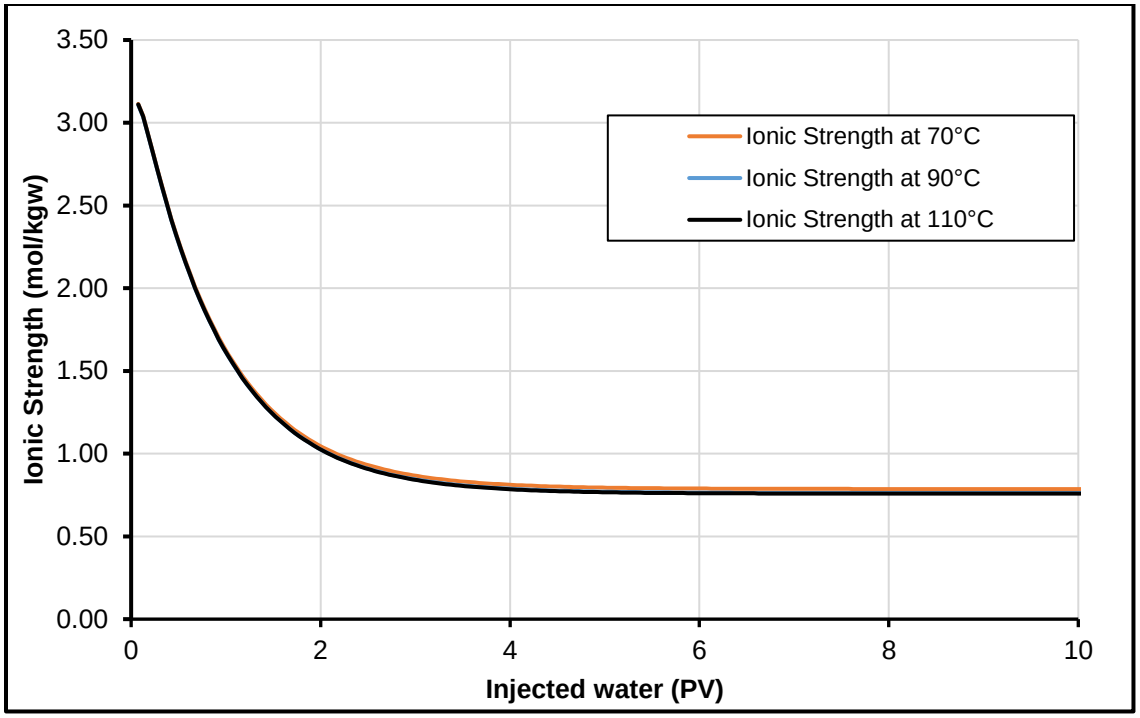

Fig. 21: Variation of ionic strength due to temperature change during seawater injection for 10 PVs.

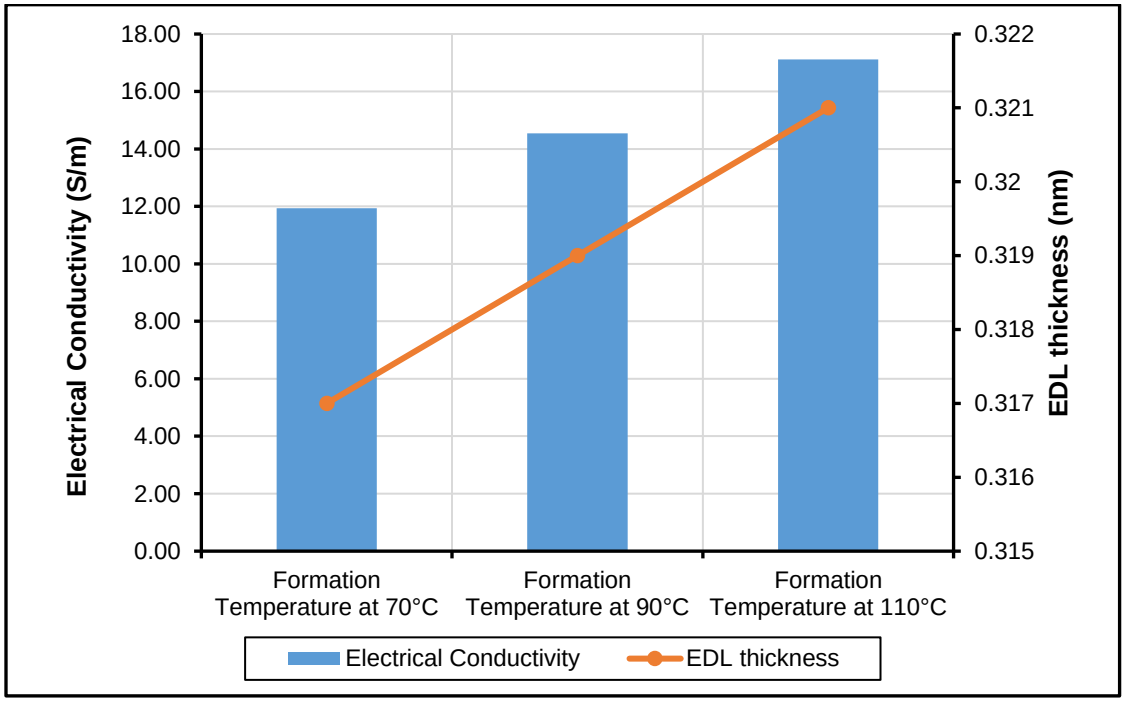

Fig. 22: Comparison of electrical conductivity and EDL thickness during seawater injection for 10 PVs at various temperatures.

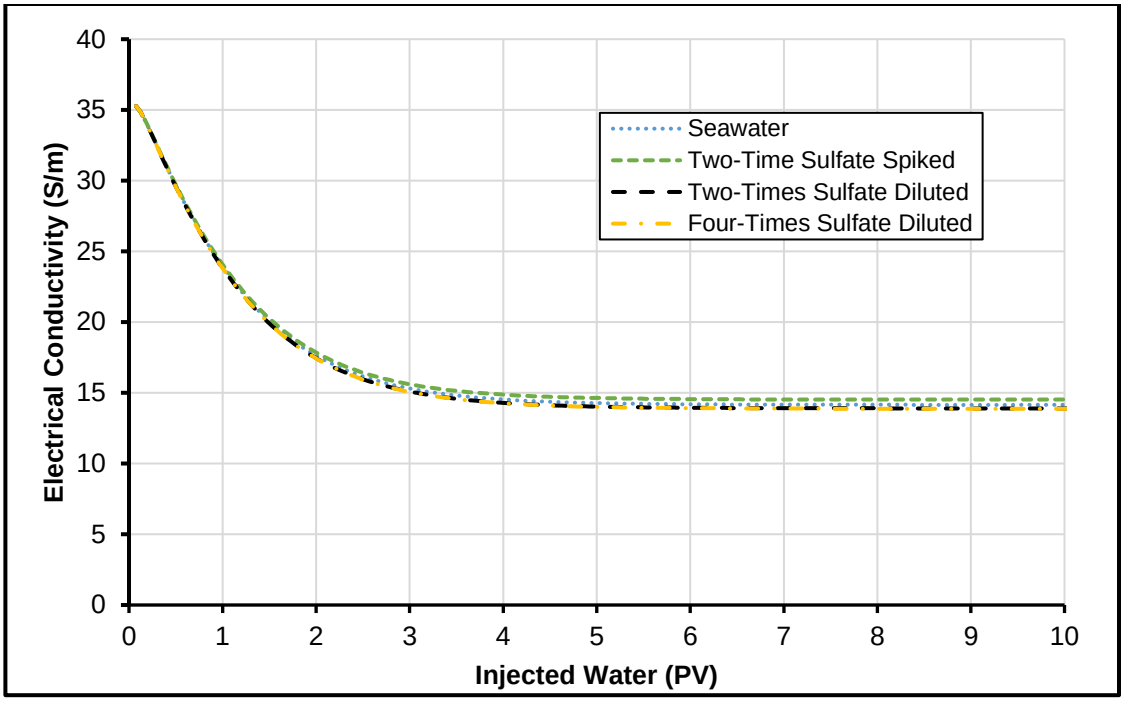

Fig. 23: Electrical conductivity change during different spiked and diluted water injections for 10 PVs at 90 ºC.

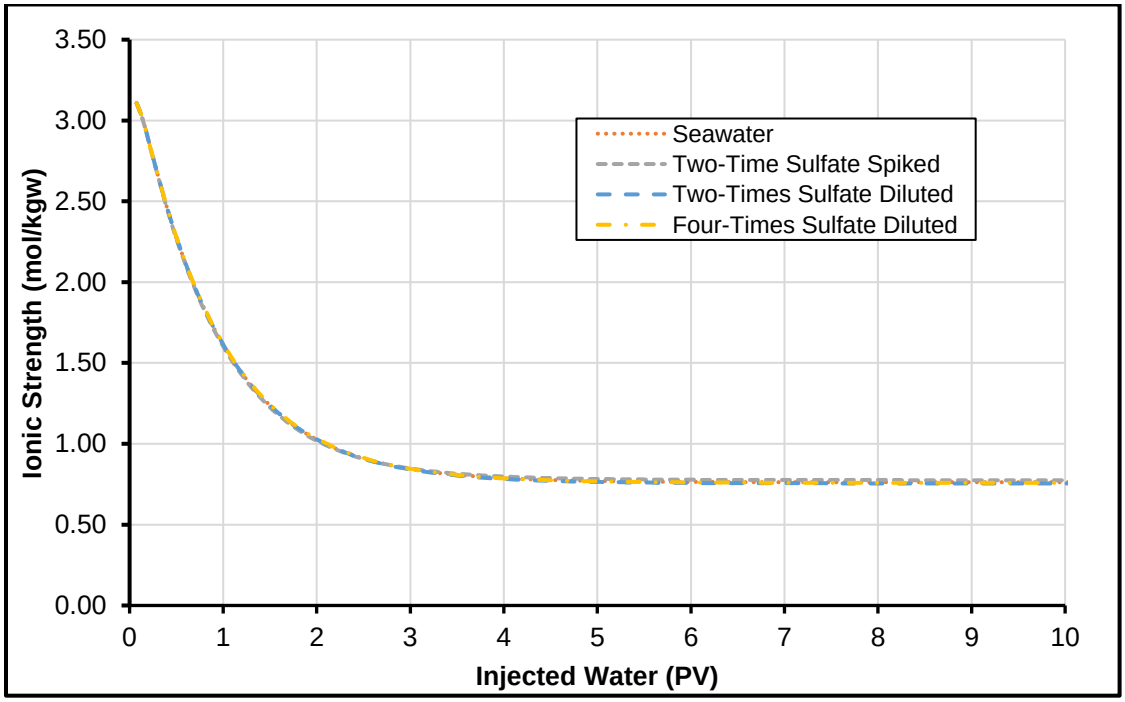

Fig. 24: Ionic strength change during different spiked and diluted water injections for 10 PVs at 90 ºC.

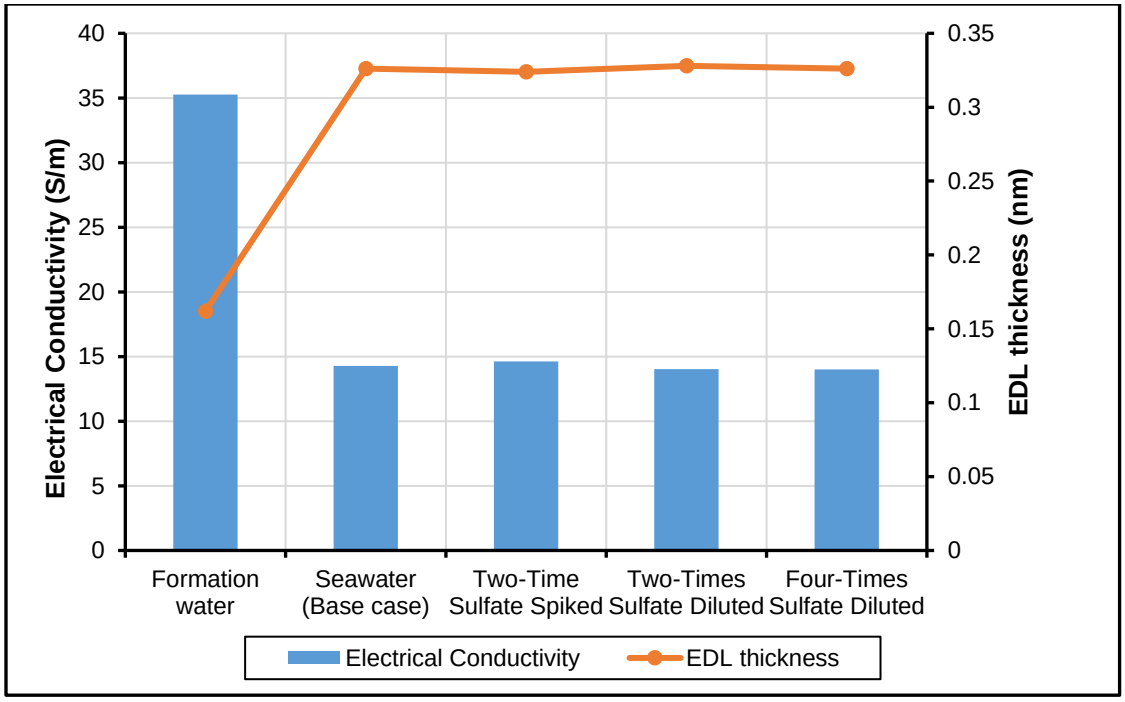

Fig. 25 Comparison of electrical conductivity and EDL thickness during different spiked and diluted water injections for 10 PVs at 90 ºC.

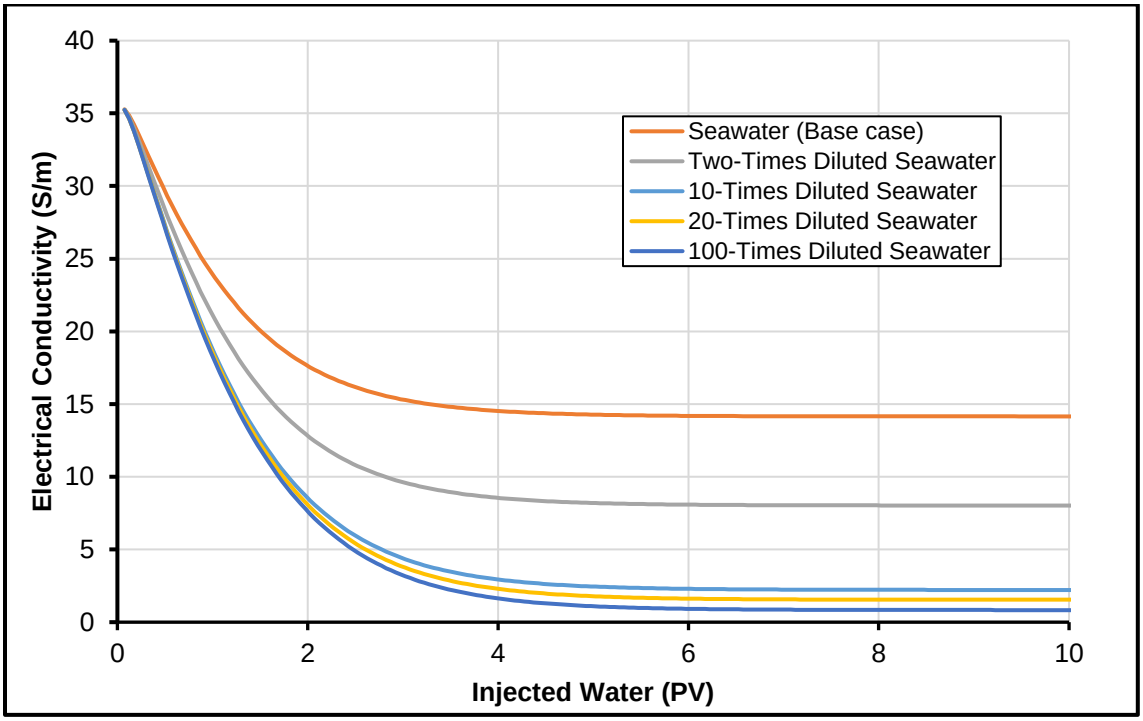

Fig. 26: Electrical conductivity change during different diluted seawater injections for 10 PVs at 90 ºC.

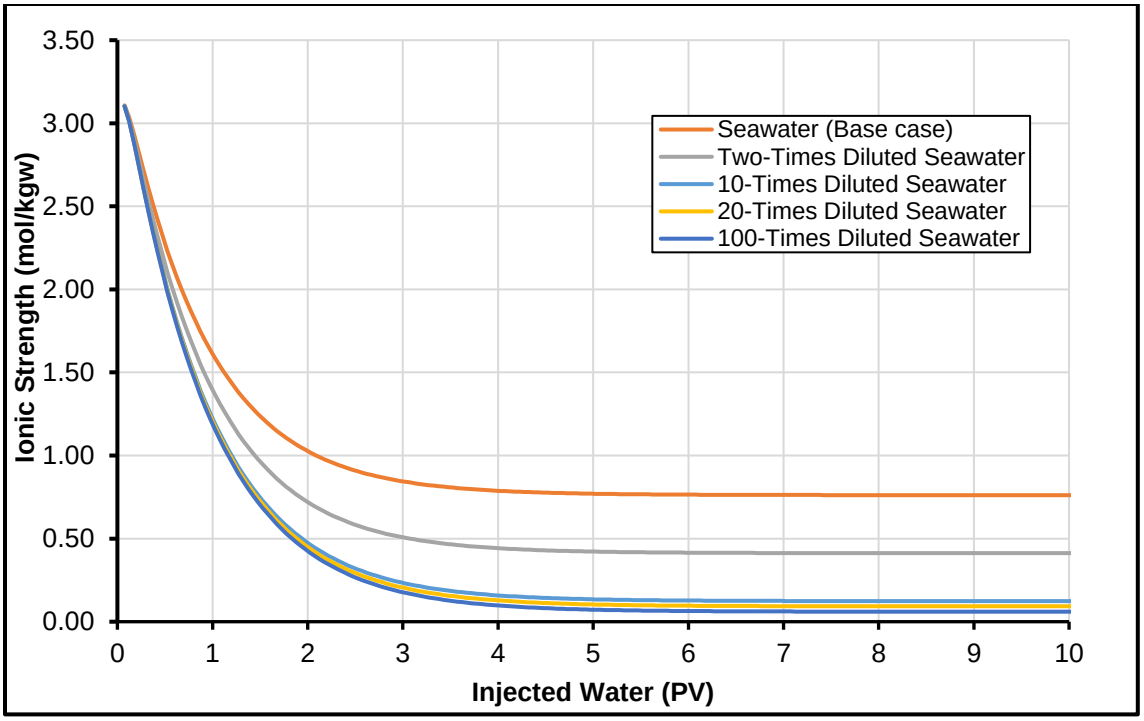

Fig. 27: Ionic strength change during different diluted seawater injections for 10 PVs at 90 ºC.

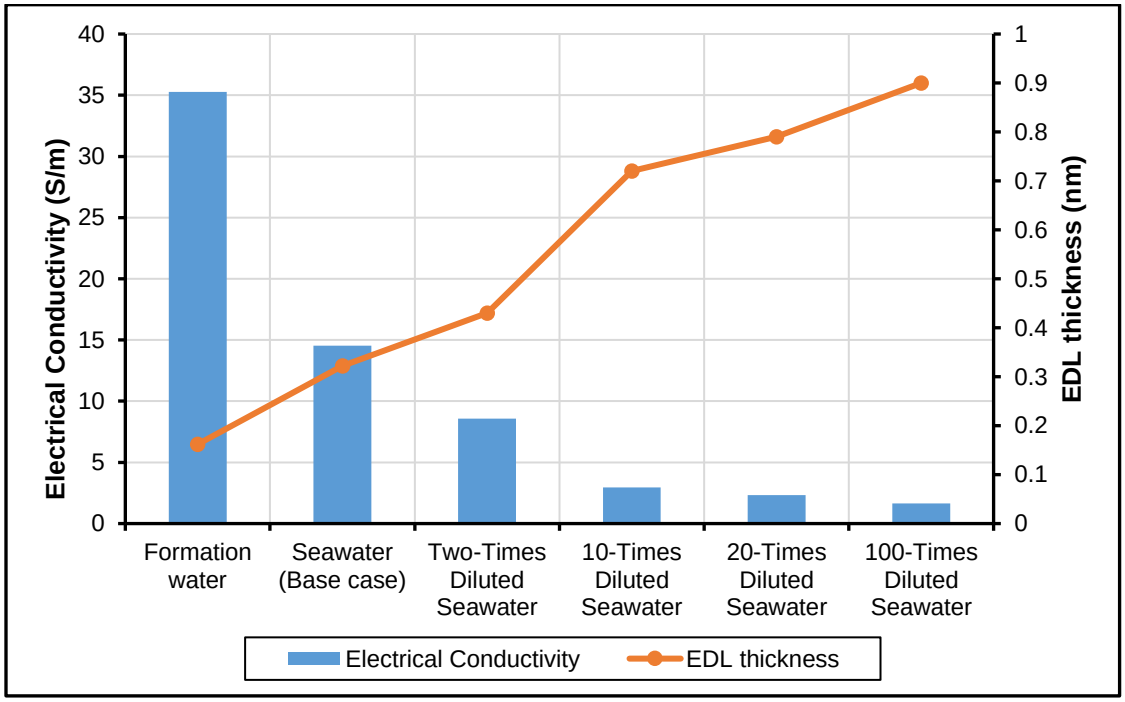

Fig. 28: Comparison of electrical conductivity and EDL thickness during different diluted seawater injections for 10 PVs at 90 ºC.

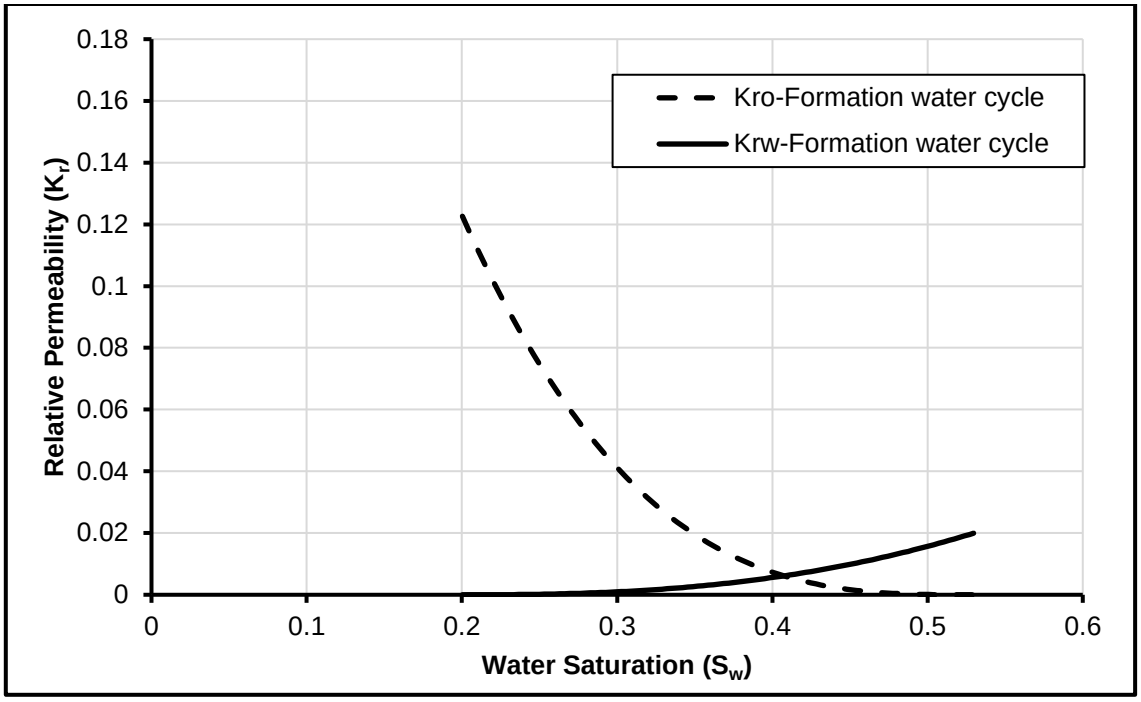

Fig. 29: Formation water relative permeability curve.

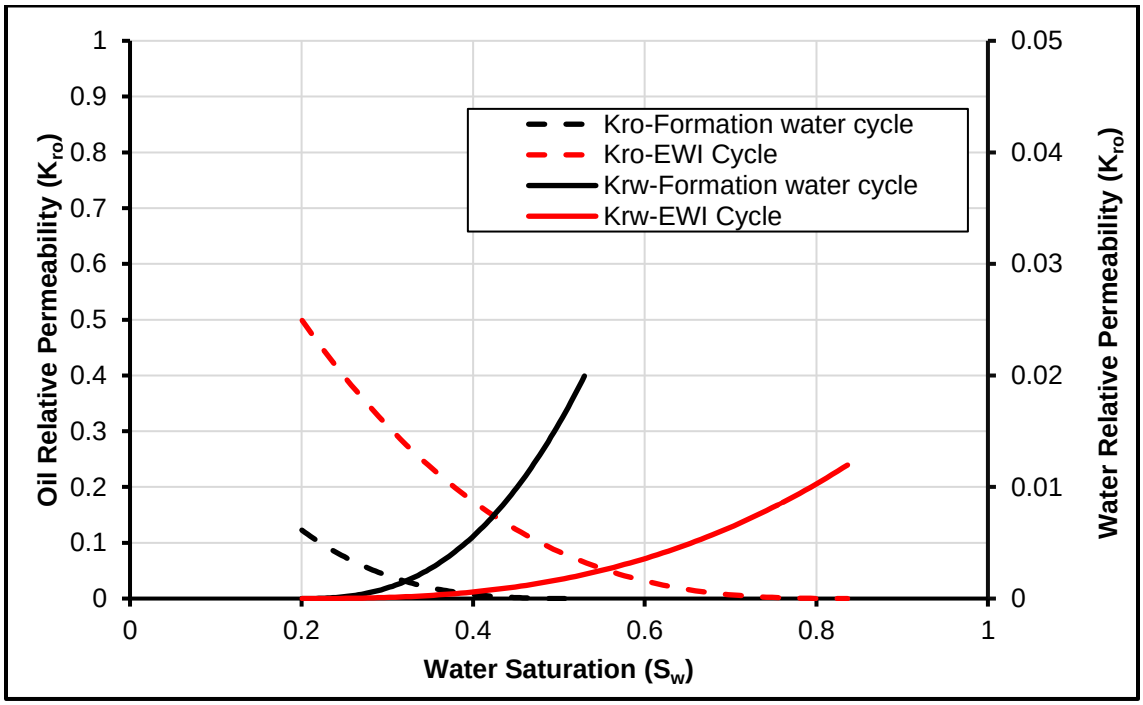

Fig. 30: Formation and engineered water relative permeability curves.

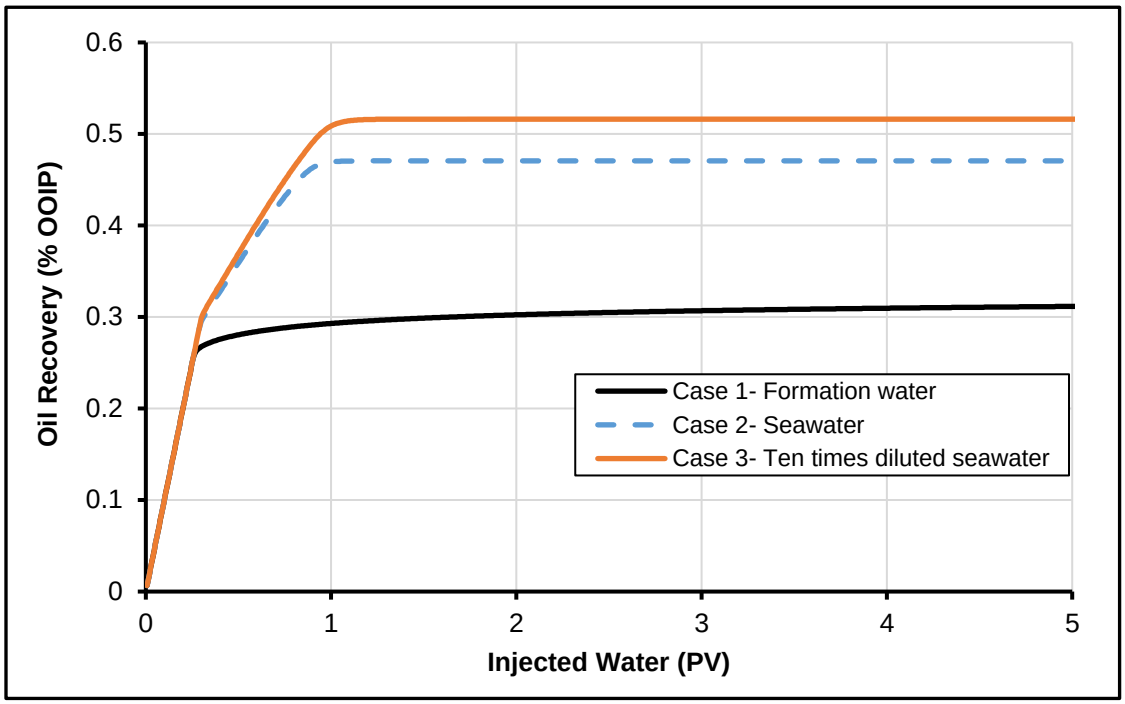

Fig. 31: Comparison of the recovery of oil at secondary EOR mode (Case 1-Formation water: no change in EC, Case 2- Seawater: with EC decreased from 35.26 S/m to 14.52 and Case 3- Ten times diluted seawater: with EC decreased from 35.26 S/m to 2.96 S/m).

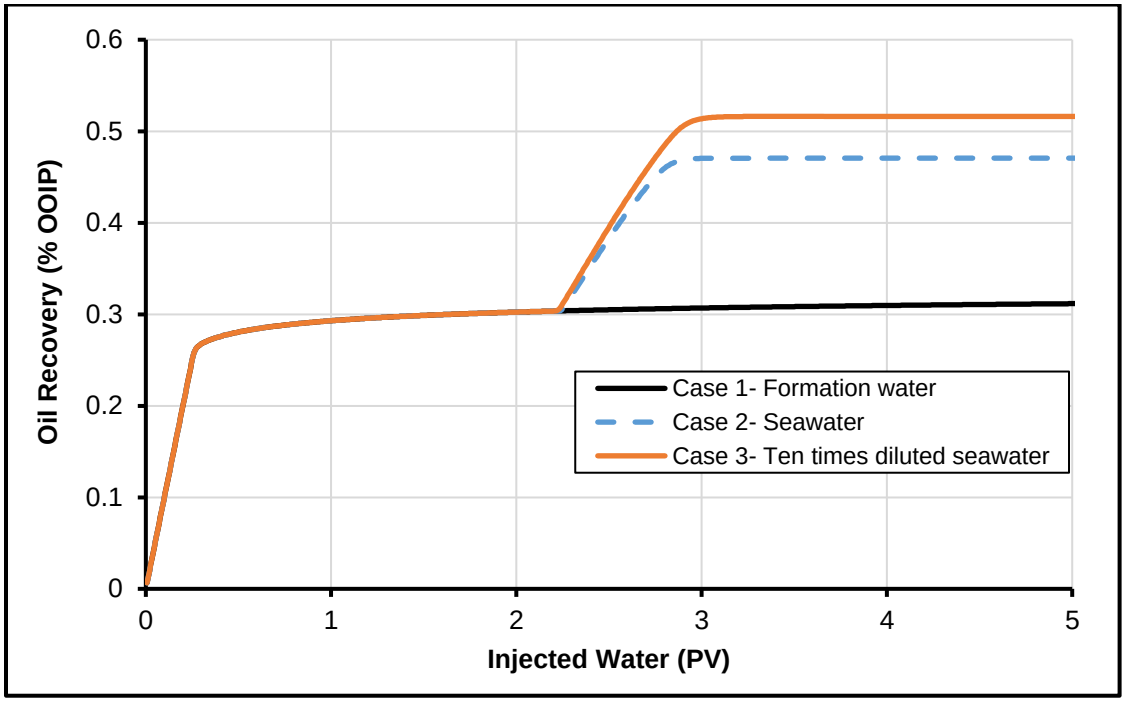

Fig. 32: Comparison of the recovery of oil at tertiary EOR mode (Case 1-Formation water: no change in EC, Case 2 - Seawater: with EC decreased from 35.26 S/m to 14.52 and Case 3 - Ten times diluted seawater: with EC decreased from 35.26 S/m to 2.96 S/m).